Fabricating and Characterization of a Metal Matrix Composite from Iron Metal Matrix Reinforced with MAX Phase V_2AlC-GO through Powder Metallurgy

Engidayehu Mekonnen Alemu

A Thesis Submitted to Department of Mechanical Engineering

College of Mechanical, Chemical and Material Engineering

Presented in Partial Fulfillment of the Requirement for the Degree of Master's in Manufacturing Engineering

Office of Graduate Studies

Adama Science and Technology University

May, 2025

Adama, Ethiopia

Fabricating and Characterization of a Metal Matrix Composite from Iron Metal Matrix Reinforced with MAX Phase V_2AlC-GO through Powder Metallurgy

Engidayehu Mekonnen Alemu

Advisor: Dr. G.M. Sayeed Ahmed (PhD)

Associate Professor

A Thesis Submitted to Department of Mechanical Engineering

College of Mechanical, Chemical and Material Engineering

Presented in Partial Fulfillment of the Requirement for the Degree of Master's in Manufacturing Engineering

Office of Graduate Studies

Adama Science and Technology University

May, 2025

Adama, Ethiopia

DECLARATION

I hereby declare that this Master Thesis entitled **"Fabricating and Characterization of a Metal Matrix Composite from Iron Metal Matrix Reinforced with MAX Phase V_2AlC-GO through Powder Metallurgy"** is my original work. That is, it has not been submitted for the award of any academic degree, diploma or certificate in any other university. All sources of materials that are used for this thesis have been duly acknowledged through citation.

Name of student	Signature	Date

RECOMMENDATION

I, the advisor of this thesis, hereby certify that I have read the revised version of the thesis entitled **"Fabricating and Characterization of a Metal Matrix Composite from Iron Metal Matrix Reinforced with MAX Phase V_2AlC-GO through Powder Metallurgy"** prepared under my guidance by Engidaheyu Mekonnen Alemu submitted in partial fulfillment of the requirements for the degree of Masters of Science in Manufacturing Engineering. Therefore, I recommend the submission of revised version of the thesis to the department following the applicable procedures.

______________________	__________	___________
Advisor	Signature	Date

APPROVAL SHEET

I, the advisor of the thesis entitled **"Fabricating and Characterization of a Metal Matrix Composite from Iron Metal Matrix Reinforced with MAX Phase V_2AlC-GO through Powder Metallurgy"** and developed by Engidaheyu Mekonnen Alemu, hereby certify that the recommendation and suggestions made by the board of examiners are appropriately incorporated into the final version of the thesis.

_________________________ ________________ ________________

Advisor Signature Date

We, the undersigned, members of the Board of Examiners of the thesis by Engidaheyu Mekonnen Alemu have read and evaluated the thesis entitled **"Fabricating and Characterization of a Metal Matrix Composite from Iron Metal Matrix Reinforced with MAX Phase V_2AlC-GO through Powder Metallurgy"** and examined the candidate during open defense. This is, therefore, to certify that the thesis is accepted for partial fulfillment of the requirement of the degree of Master of Science in Manufacturing Engineering.

_______________________ _______________ ____________________

Chairperson Signature Date

Dr.Moera Gutu 05/06/2025

Internal Examiner Signature Date

_______________________ _______________ ____________________

External Examiner Signature Date

Final approval and acceptance of the thesis is contingent upon submission of its final copy to the Office of Postgraduate Studies (OPGS) through the Department Graduate Council (DGC) and College Graduate Committee (CGC).

_________________________ _______________ ________________

Department Head Signature Date

_________________________ _______________ ________________

College Dean Signature Date

_________________________ _______________ _______________

Office of Postgraduate Studies Dean Signature Date

ACKNOWLEDGEMENT

I praise God, the Almighty, for providing me this opportunity. Next to that, I would like to express my deep sense of respect and gratitude to Dr. G.M. Sayeed Ahmed (PhD), my supervisor, for his invaluable and fruitful constructive suggestions and guidance that have enabled me to overcome all the problems and difficulties while carrying out this study. He stayed along with me and motivated me constantly and stimulated me to the fullest extent. I feel fortunate for his support and involvement, and this is virtually impossible to express in words. I also express my gratitude to Dr. Devendra Kumar Sinha for his valuable comments and advice during this study. Thanks for providing me with the required material for this study at no charge. I would like to express my deepest gratitude to the ASTU Material Science and Engineering department and their laboratory assistance for their invaluable support throughout this research. Their expertise, guidance, and resources have been instrumental in the successful completion of this study.

TABLE OF CONTENTS

LIST OF TABLES

LIST OF FIGURES

ACRONYMS AND ABBREVIATIONS

ANOVA	Analysis Of Variance
ASTM	American Society for Testing Materials
CP	Compacting Pressure
Ecorr	Corrosion Potential
GRA	Grey Relation Analysis
HV	Vickers Hardness
Icorr	Corrosion Current
IMMC	Iron Metal Matrix Composite
MMC	Metal Matrix Composites
MT	Milling Time
OM	Optical Microscope
PDF	Powder Diffraction File
PM	Powder Metallurgy
RF	Reinforcement
ST	Sintering Temperature
UTM	Universal Testing Machine
XRD	X-Ray Diffraction

ABSTRACT

Due to rapid modernization and technological advancements, the development of high-quality composites has become increasingly important. In the current era of rapid material advancement, traditional iron-based materials face significant limitations, including high density, low strength-to-weight ratio, and poor corrosion and wear resistance. This research focuses on fabricating a metal matrix composite from a pure iron metal matrix reinforced with vanadium aluminum carbide and graphene oxide as dry lubricant using the powder metallurgy method and testing its mechanical properties. Optical Microscope (OM) and X-ray diffraction (XRD) were used for characterization of the microstructure of the sample. The Archimedes principle was used to determine the density and porosity of the sample. Analyses of hardness, compressive strength, and corrosion resistance were performed as per ASTM standard. The corrosion resistance of the samples was investigated using an electrochemical analyzer. At the first, nine samples were fabricated from 5 wt.% vanadium aluminum carbide and 4 wt.% graphene-oxide by varying powder metallurgy process parameters. Based on these samples, the process parameters of powder metallurgy were optimized using Taguchi-based grey relational analysis (GRA). After determining the optimal process parameter, an additional four samples (5 wt.%, 8 wt.%, 10 wt.% and 15 wt.%) were created by varying the weight percentage of vanadium aluminum carbide. The significant improvement of physical, mechanical, and corrosion resistance properties were obtained from the optimally fabricated sample. The OM characterization result showed uniform distribution of reinforcements throughout the matrix. The XRD test confirmed the presence of different phases in the composite. The addition of vanadium aluminum carbide reinforcements to the iron matrix has improved its physical, mechanical, and corrosion resistance properties, the optimal composite sample (Fe-10 V_2AlC-GO) the achived results were density of 6.983 g/cm^3, hardness of 534.2 HV and compressieve strength of 702MPa. Hence, newly developed iron metal matrix composite was expected to be used in the construction, automotive, aerospace, and marine industries.

Key words: *Iron metal matrix composite, vanadium aluminum carbide, GRA, mechanical properties, powder metallurgy.*

CHAPTER ONE: INTRODUCTION

1.1 Background of the Study

The production and innovation of advanced materials that satisfy the requirements of developing new applications is an essential area of study in the manufacturing industry. Because of today's rapid modernization and advancements, the development of high-quality alloys is becoming a crucial issue to fulfill the interesting, and the implementation of smart materials for successfully completing various tasks in terms of weight, strength, strength-to-weight ratio, and cost minimization has been increasing (Aydogmus, 2015; Singh et al., 2022). Over the past few decades, materials development has shifted from monolithic to composite materials in order to meet the global need (P. S. Sahu & Banchhor, 2016). With technological progress in the present world, monolithic materials are no longer able to satisfy to meet the increasing demands on product capabilities and functions. This incapability has led to the development of some advanced materials which can serve with better structural, mechanical and electrochemical properties (Gupta et al., 2015).

A composite material is made up of elements that are produced by mechanically combining pre-existing ingredient materials to manufacture a new material with special properties when compared to monolithic material properties. Metal matrix composites (MMC) are a type of composite material fabricated by mixing two or more components that have superior qualities to the individual components (the matrix phase). Reinforcing elements in metal matrix composites (MMC) typically include ceramic whiskers, continuous or discontinuous fibers, and particles (Chauhan et al., 2017; Öksüz et al., 2014). Based on the size and shape of the reinforcement material, metal matrix composites can be, classified as whiskers, monofilament and particles. The shape and size of the reinforcement affect the properties of the produce material and different manufacturing method is, needed. Powder form of reinforcements can be termed as particulates.

Metal Matrix Nanocomposites (MMNCs) is one type of advanced material which possesses significantly improved properties including higher specific strength, specific modulus, damping capacity, wear resistance and corrosion resistance compared to unreinforced alloys. Metal matrix composites (MMCs) are defined as a class of composite materials that employ hard and brittle ceramic reinforcements such as Aluminum Oxide (Al_2O_3), Silicon Carbide (SiC) and Tungsten Carbide (WC) in ductile metallic matrix such as Al, Cu and Mg (Jha et al., 2014). Metal Matrix Composites are the most promising materials and find their usage in a wide range of industrial application such as automotive, aerospace, defense, marine, and electronics (Samal et al., 2023). Containing hard particulates offer superior operating performance and resistance to wear. In industrial processes elements fabricated from MMC materials give higher abrasive resistance and so a longer service life.

Iron based reinforced MMCs are in demand due to their improved strength, high modulus, and increased wear resistance over conventional Fe alloys, have better values of structural and mechanical properties (Jha et al., 2014; Yılmaz, 2001). Wrought iron, structural steel, and mild steel are commonly used iron-based metals in construction in Ethiopia (e.g., for stairs, columns, beams, window frames, gates, and doors). However, they are prone to corrosion when exposed to moisture and oxygen.

There are various methods for the fabrication of the quality MMC products. These include stir casting, Powder Metallurgy (PM), Physical Vapor Deposition (PVD), Chemical Vapor Deposition (CVD) etc. Among these PM technique is used to fabricate quality MMC products with more near net shaped object with utmost dimensional accuracy (Gupta et al., 2015).

1.2 Statement of the Problem

In today's developed environment, the discovery of new materials is evolving at a rapid rate. Short life, low strength-to-weight ratio, low corrosion resistance, and increased density are all issues in this regard. Iron form of material is widely used for structural support in construction. It is used in the fabrication of beams, columns, girders, and other structural components to provide strength and stability to buildings, bridges, and infrastructure projects and also used in the manufacturing of engine blocks, cylinder heads, crankshafts, and other critical parts of automobiles. Iron is highly susceptible to corrosion, particularly in the presence of moisture and oxygen, when it is exposed to water it easily corroded because of its inherent reactivity and the tendency to form less stable, non-protective oxides when exposed to moisture and oxygen. This leads to a continuous oxidation process, weakening the iron structure and resulting in rust. Pure iron has a relatively low resistance to high temperatures. It tends to soften and lose strength at elevated temperatures. For example wrought iron has been used in various applications, including gates, fences, railings, window grills (window frames), staircases, furniture, etc.

Wrought iron has better corrosion resistance compared to other forms of iron, it is still susceptible to rust and corrosion, especially in harsh environments or when not properly maintained, regular inspections and protective coatings are necessary to prevent deterioration and also structural steels are used for beam in construction, Structural steel is prone to corrosion when exposed to moisture and oxygen. Over time, this can lead to rust formation, weakening the material and compromising its structural integrity.

Wrought iron and Structural steels are denser and heavier than many other construction materials. This increased weight can affect transportation and installation processes, requiring specialized equipment and additional logistical considerations. Therefore, lots of challenges are being faced by construction and other industries where Iron finds applications.

In Ethiopia, mild steel is commonly used for toilet doors, but it is highly prone to corrosion, especially when exposed to acidic moisture. This leads to frequent maintenance, increased costs, and a short service life for the doors. Therefore, there is a need to improve the mechanical and corrosion resistance properties of iron-based materials. This study focuses on enhancing the physical, mechanical, and corrosion behavior of an iron metal matrix reinforced with V_2AlC-GO to address those challenges.

1.3 Research Questions

1. What are the most significant process parameters during fabrication in powder metallurgy?
2. For which selection of process parameters the best mechanical and metallurgical characteristics of iron composites material was achieved?
3. For which percentage of reinforcement the average, better and acceptable properties of the sample were achieved?
4. At what percentage of reinforcement the corrosive resistance iron matrices composites was achieved?

1.4 Objectives of the Study

1.4.1General objective

The general objective of the study is to fabricate, investigate PM process parameters, optimization and analysis physical and mechanical properties of Iron metal matrix reinforced with V_2AlC MAX phase.

1.4.2 Specific objectives

1. To fabricate and analyze the effect of powder metallurgy parameters such as, milling time, compaction pressure, sintering temperature on physical and mechanical properties.
2. To optimize intput values of powder metallurgy parameters such as, milling time compaction pressure, sintering temperature using Taguchi based GRA baesd on physical and mechanical properties of the developed samples.
3. To analyze the effect of weight percentage of reinforcement on Iron metal matrix reinforced with V_2AlC MAX phase with optimal parameter.
4. To investigate corrosion behavior of developed samples.
5. To characterize phase, morphology and crystalline size of the developed samples.

1.5 Significance of the Study

Modern manufacturing sectors, like the aerospace, construction and automobile industries, have a great need for stronger, lighter components made of affordable composite materials. In order to improve the corrosion and wear resistance of Fe-V_2AlC reinforced metal matrix composites, it is important to fabricate, characterize, and evaluate their mechanical properties. The study focuses on the corrosion resistance and service life of composites by reducing the weight of industrial, construction and automotive components. Longer-lasting materials can be generated by improving the mechanical and physical properties of the samples and knowing how to prevent porosity in them. Because of this, this research serves as inspiration and a crucial tool for converting my theoretical understanding into actual reality. Therefore, it has crucial benefit for individuals as well as other stakeholders at the national and international levels both academically and practically. Additionally it will have importance for current and future researchers it will enhance their theoretical and practical understanding of the topic. The developed composite material will be the potential candidate for use in construction (particularly for application of window frames, beams and stairs), and applications where specific weights to strength ratio, hardness, compressive strength and corrosion resistance are of major concern.

1.6 Scope of the Study

This thesis were focus on fabricated samples, study effects of powder metallurgy parameters, characterization, and multi-objective parametric optimization of iron metal reinforced with V_2AlC. Samples were fabricated through powder metallurgy. Mechanical properties (hardness, compression strength) and corrosion properties of the developed sample were investigated. A verity of experiment and testing were conducted for this study including investigation of hardness test, corrosion test, compression strength test and characterization of the developed samples were conducted with X-RD and OM. The optimum process parameter determined through Taguchi based GRA. The appealing features of Fe-V_2AlC-GO composites make them appealing for a wide range of construction (such as gates, fences, beams and toilet doors applications).

1.7 Research Motivation

Researchers can no longer create and study reinforced iron-based metal matrix composites because of their high damage and low corrosion properties. It is possible to produce composites with marginally improved mechanical and metallurgical properties. Consequently, controlling and enhancing the mechanical and metallurgical performance of the generated composites is the main focus of this investigation. When clever reinforcing composites (MAX phase) like V_2AlC and Graphene Oxide as lubricant are added, the basic matrix's mechanical and metallurgical qualities get better.

1.8 Limitations for the Study

Here is a list of the limitations encountered in this study when producing the samples:

- ❖ The resources' accessibility and the lab groups' cooperative spirit.
- ❖ The equipment and facilities employed for the test and experiment's availability and effectiveness.
- ❖ In addition, the installation of the machine for the particular task and the need for a qualified worker.

1.9 Thesis Organizations

The overall structure of this document can be summarized as follows:

This study is organized and categorized using thorough plans for accomplishing the particular objective as explained in the chapters. In chapter one, the research focused on the introduction including background of the study, statement of the problem, research questions, objectives of the study, research scope, research motivations and research limitations. And, Chapter two reviews several literature types according to the significance of the study as well as the approaches and designs used to highlight issues brought up in earlier research. In chapter three, in order to explore the impact of input process parameters (namely, the ratio of matrix and reinforcement, milling time, compaction pressure, and sintering temperature) on mechanical properties, specifically hardness, compression, density, and porosity properties on the fabricated sample of MMCs, a brief description of the materials and methods is provided. This includes conducting an experiment using PM after sample preparation and going through the testing procedures. It deals with applying the Taguchi-based GRA multi-objective optimization method to determine the best possible combination of process parameters. Additionally, it concentrates on evaluating the improved samples' mechanical, metallurgical (microstructure), and corrosion resistance qualities. Chapter Four provides an interpretation and brief discussion of the results, which come from various tests. It also highlights the study's limits, significance, and recommendations for further research. Chapter five concludes and summarizes the findings by comparing the outcomes to the scraps of evidence in the review section.

CHAPTER TWO: LITERATURE REVIEW

2.1 Introduction

In a composite material, Metal matrix composites are recognized after more than a quarter of a century of active research. MMCs comprise a metal as a matrix and other material as a dispersed phase. In this chapter, the literatures was taken to review about the matrix, reinforcing materials, manufacturing method (i.e. powder metallurgy, stir casting and others), process parameters of manufacturing method, properties of MMCs, and data analysis methods.

2.2 Composite Materials and MAX Phases

A composite material system consists of a proper combination or mixing of two or more macro and micro components that are separated by interfaces yet have different shapes and chemical compositions. When a material combines a significant amount of the characteristics of the matrix component (which contains the continuous phase) and the reinforcing phase (which contains the discrete components), it develop a composite material that has a superior combination of properties (Bodunrin et al., 2015; Mavhungu et al., 2017). This composite material has exhibit fatigue, and wear and corrosion resistance as well as a high strength-to-weight and modulus-to-weight ratio. These applications require materials with higher specific strength, hardness, wear resistance, and dimensional stability at high temperatures.

The distribution, their interactions, and characteristics of their constituents all have a great impact on the properties of composite materials. In addition to the type of beginning material, the morphology of the reinforcement (shape, size, and particle distribution) has a significant effect on the composite properties. The orientation and concentration distribution of the reinforcement dictate how each component contributes to the overall properties of the composite. Among the many MMCs, non-ferrous matrix composites (NFMMCs) constitute an important application field (Singh et al., 2022).

But among the numerous MMCs, heavy-duty road vehicles and railroads (NFMMCs) are a major application arena where the consistency of FMMC research has been conducted (Paswan et al., 2021). To prevent oxidation and reactivity with strengthening agents, great vigilance is required during the synthesis of FMMC. By conserving resources including materials, energy, and post-processing, lower temperature requirements in the PM range protect ferrous materials against interactions with reinforcements and the environment. In order to suit the demanding applications in aerospace, automotive, marine, sports, and bio-implants, MMCs have emerged as a new class of materials throughout the previous two decades (Singh et al., 2022).

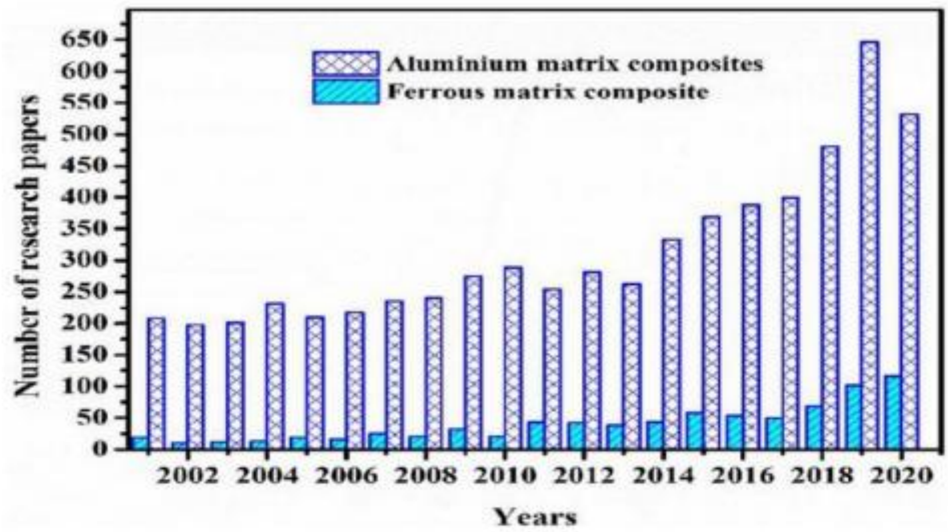

Figure 2.1 Number Research's Paper Per Year (Singh et al., 2022).

Until 2019, the number of research articles on ferrous matrix-based composites was six to eight times lower than that on aluminum matrix-based composites. However, aluminum composites have shown a minor downturn in 2020. This data clearly shows that more research articles are being released each year, which is advantageous for composites based on ferrous matrices.

MAX phase materials are a new family of ternary layered carbide and nitride compounds are represented by the general formula of Mn+1AXn, where $n = 1 \sim 3$. A stands for A-group elements, M for early transition metal, and X can be either nitrogen or carbon. Ceramics in the MAX phase have applications in both structural and functional fields, and they are thought to be the best strengthening phase for metal matrix composites. Researchers have identified the areas in which this novel material may find significant technological applications, including nuclear power, high-speed rail, gas igniters, heat exchangers, high thrust rocket nozzles, electric brushes, kiln furnishings, metal refining electrodes, and high-temperature seals (Lei & Lin, 2022).

2.3 Metal matrix composite

Metal matrix composites (MMC) are lightweight, have a sound surface, and have mechanical properties that make them useful in many manufacturing applications. Its useful applications in the fields of space and defense make it worthwhile to investigate for potential low-cost and user-friendly solutions (S. Kumar et al., 2020). Metal matrix composites are new materials with appealing technical properties of their own that are created by combining a metal with another, sometimes nonmetallic, phase (Mortensen & Llorca, 2010).

A common aluminum matrix with a variety of reinforcements, including oxides, carbides and borides, nitrides, and fly ash, is the foundation for most MMCs developed to date. Almost all NFMMC applications, ranging from satellite launchers to road transportation vehicles, are dominated by aluminum-based MMCs. Ferrous metal matrix composites are a viable option for both road and airplane transportation, in addition to non-ferrous metal matrix composites. The assumption that aluminum matrix composites were the most common was confirmed by the graphical display of data gathered from the Web of Science.

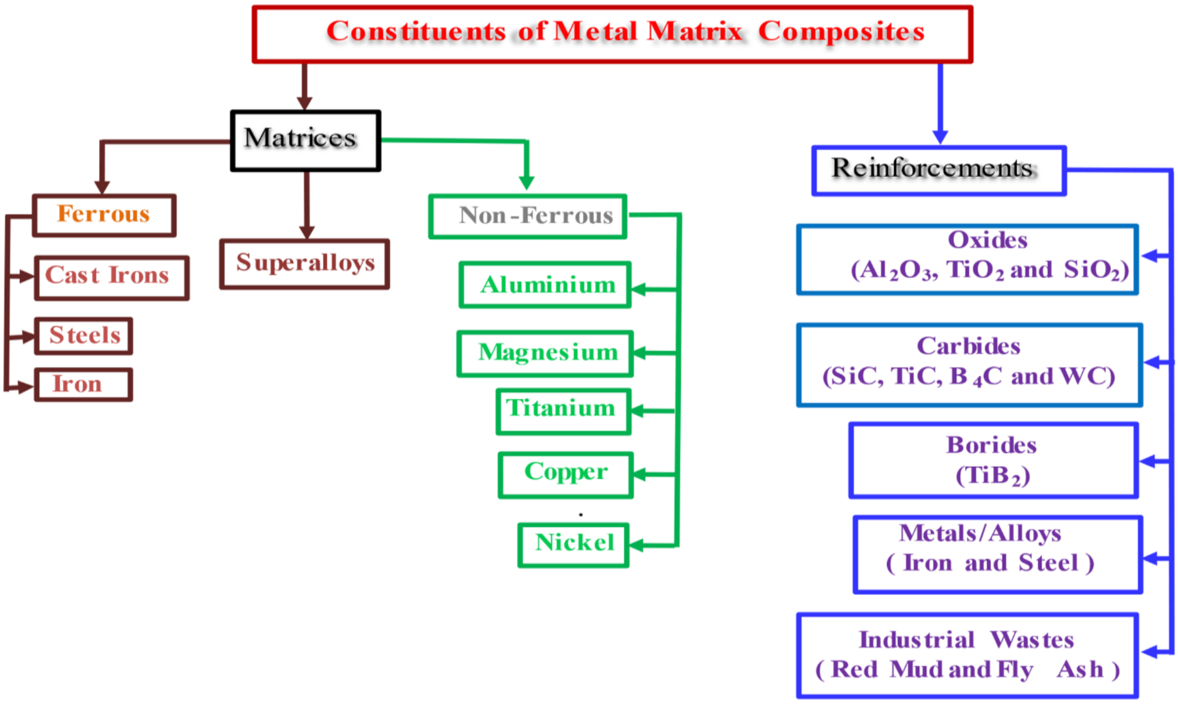

Figure 2.2 Classification of MMC's (Singh et al., 2023).

2.4 Ferrous Metal Matrix Composites (FMMC's)

The FMMCs are older but relatively few in application as compared to the non-ferrous metal matrix composites (NFMMCs). Powder metallurgy is the widely used process for fabricating iron and steel-based FMMCs by reinforcing particulates. At the same time, the in-situ method has been used for the fabrication of cast iron-based FMMCs. The main characteristics considered during the designing and the fabrication of FMMCs are wear resistance and improved specific mechanical properties (Singh et al., 2023).

2.4.1 Iron based metal matrix composites

Iron is an essential substance in physical metallurgy because it can be alloyed with other elements to produce well-known products like steels and super alloys. Iron-based metal matrix composites with superior physical, mechanical, and tribological properties have recently been created and successfully used in a variety of areas including automotive, aerospace, sports, and rail transportation. During this age of tremendous growth, research seeks to investigate alternatives to traditional materials. Metal matrix composites have enormous potential because they can impart characteristics that traditional alloys cannot.

Several iron-based composites have been studied to improve their mechanical and tribological properties at varying weights. Different reinforcements are used in wt.%. The most related works are described here:

2.4.1.1 Microstructural and mechanical properties of IMMC's

(Meher et al., 2021) studied the effects of wet and dry milling on the phase transformation, microstructure evolution and mechanical properties during fabrication of iron based composite reinforced with 21 vol% MWCNTs (Multi-Walled Carbon Nanotubes) by using high energy planetary milling followed by pressureless conventional sintering. A powder mixture containing Fe-21 vol% MWCNTs was milled in both wet (toluene) and dry (argon atmosphere) condition for 12 h in a dual drive planetary mill. The maximum hardness of 450 VHN and compressive strength of 525 MPa were achieved for the wet milled composite powders sintered at 1300 °C for 2 h.

(Jha et al., 2015) investigated microstructure, and compressive strength of ZrO_2 reinforced Fe Metal Matrix Nanocomposites (MMNCs) synthesized by powder metallurgy technique. High purity grade iron metal powder was mixed with varying percentage of Zirconium dioxide (5–30 wt%), compacted, and sintered in argon atmosphere in the temperature range of 900–1100 °C for 1 to 3 hours. X-ray diffraction (XRD) analysis of specimens was done in order to study the phases present and scanning electron microscopy was carried out to determine the morphology and grain size of the various constituents. XRD result shows the presence of Fe, ZrO_2, and $Zr6Fe_3O$ phase. $Zr6Fe_3O$ phase forms due to reactive sintering and is not reported earlier by researchers throughout the globe. SEM results showed the presence of dense microstructure with the presence of Fe, ZrO_2, and some nanosize $Zr6Fe_3O$ phases.

(Gupta et al., 2014) studied on sintering and hardness behavior of Fe- Al_2O_3 Metal Matrix Nanocomposites (MMNCs) prepared by powder metallurgy route with varying concentration of Al_2O_3 (5–30 wt%). The MMNC specimens for the present investigations were synthesized by ball milling, followed by compaction and sintering in an inert atmosphere in the temperature range of 900–1100∘ C for 1–3 hours using Powder Metallurgy route. For the sintering of the specimen done at 900∘ C for 1 h and 2 h of time interval, the hardness value first increases up to 10 wt% of Al_2O_3 and then it decreases for 20 wt%. For 3 h of time interval at 900∘ C the hardness increases with the content of reinforcement. It is due to the reason that at this temperature and time interval optimum amount of iron aluminate phase formation has taken place. The hardness values for the specimen sintered at 1000∘ C and 1100∘ C for different time intervals showed a continuous increase in the hardness values up to 20% of Al_2O_3 reinforcement. The hardness for the 30% reinforced Al_2O_3 could not be found due to brittleness of the specimen. It was found from the investigations that the ductility is maintained in the specimens up to 10% of the aluminum oxide dispersion after which the specimens become brittle in nature which is due to the increase in the formation of iron aluminate phase.

(Shivakumar et al., 2020) investigated the mechanical properties of the aluminum matrix composites. The aluminum 6061 alloy as a matrix reinforced with the weight fraction 2, 4 and 6% of particles of iron oxide (Fe_2O_3) of size 40μm is prepared using the stir casting technique. The prepared specimens are tested as per the standards for tensile, bending, impact and hardness properties of the composite. From the results it is observed that the mechanical properties of the said composite have increased with the increment in the weight percentage of iron oxide up to 4% of reinforcement. The tensile strength obtained by the adding the 4 wt%, 5 wt% and 10 wt% of SiC particles to the aluminum alloy improves the tensile strength by 20.38%, 3.81% and 6.25% respectively in contrast with the unreinforced aluminum alloy.

(Tugirumubano et al., 2021) fabricated and characterized the aluminum metal matrix composites reinforced with carbon nanotube, iron and nickel nanoparticles were fabricated using ball milling followed by spark plasma sintering. The 80 vol%, 75 vol% and 70 vol% of aluminum matrix reinforced with Fe (16 – 28 vol%), MWCNT 2 vol% and Ni (0–2 vol%) were considered. The composites were characterized for the magnetic properties using VSM and toroid measurements. The particles distribution and microstructure of the composites were observed through OM and SEM. The spark plasma sintered aluminum metal matrix composites exhibited ferromagnetic character, even at lower content as 18 vol% of ferromagnetic reinforcement in aluminum matrix.

(Bahari et al., 2012) studied Al-Fe-Cr-Ti nanocomposite structures using XRD and AFM techniques. It obviously depends on the manufacturing method and the combination of Ti and Al content. Acetic acid was added to the solvent over 30 minutes at room temperature. This solution was then mixed with titanium chlorides TiCl4, Al2O3, Fe2O3, and FeCr2O4 at 0 °C in specific molar ratios to obtain different contents. The sol was stirred at 60° C. until it gelled and ethanol was removed (approximately 24 hours). The temperature gradient during the test run was 5 degrees/minute and the samples were placed in the oven for 2 hours at various firing temperatures. The obtained results from XRD (X-ray Diffraction), AFM (Atomic Force Microscopy) and X-ray powder techniques indicate that nano-grains with 0.03 at %Cr can cause a reduction of leakage current through the SS chamber due to its amorphous structure.

(Chauhan et al., 2017) were conducted research on induction hardening of powder metallurgically treated Fe-Cr/Mo alloys. Pre-alloyed powders Fe-3Cr-0.5Mo, Fe-1.5Cr-0.2Mo and Fe-0.85Mo 15 were mixed at 0.4 wt%, 0.6 wt% and 0.8 wt% and tested by compression at 500, 600 and 700 MPa. bottom. Alternatively, the compacts were sintered at 1473 K for 1 hour and then cooled at 6 K/min. Hardness varied from HV 600 to HV 375 from the surface of the sample to the interior of the casehardened region. The best combination of properties and hardening depth was achieved for Fe1.5Cr-0.2Mo alloy with 0.6 wt% C. A 0.6 wt% sintered Fe-1.5Cr-0.2Mo alloy has a high tensile strength of 457.7 MPa, an elongation of 6.4% and a hardness of HV 233. The maximum hardness of the alloy after induction hardening is HV 600. The case depth is 2.5 mm. Therefore, among the studied alloys, the Fe-1.5Cr-0.2Mo alloy containing 0.6 wt% C is the most suitable for automotive gears and engine parts.

(Jha et al., 2014) investigated microstructure and hardness of ZrO_2-reinforced iron-based metal matrix composites synthesized by powder metallurgy. The process involved the preparation of homogeneous mixture of electrolytic iron powder with different weight percentages (5%, 10%, 20% and 30%) of ZrO_2 by milling, compaction in the form of rod and sintering in the temperature range of 900–1100°C for 1–3 h in argon atmosphere. The sintered samples were subjected to X-ray diffraction for phase analysis and to scanning electron microscopy for microstructure evaluation. The X-ray diffraction and scanning electron microscopy results show the presence of Fe, ZrO_2 and $Zr6Fe_3O$ phases. This Zr_6Fe_3O phase is formed due to reactive sintering. From these studies it is concluded that two types of sintering are involved: (a) solid state sintering between Fe particles and (b) reactive sintering with the formation of iron zirconium oxide. Density and hardness of composite specimens were found to depend on fraction of ZrO_2, the nature of sintering and the formation of Zr_6Fe_3O phases.

2.4.1.2 Corrosion and tribological behavior of reinforced IMMC's

(C. Li et al., 2022) investigated interfacial characteristics and abrasive wear behaviors of Zirconia-Toughened Alumina ceramic particle (ZTA_P)/Fe composites. Results showed that sintering played a significant role in the formation of sintering necks and consequently affected both compressive strengths and porosities of ZTA ceramic preforms. Optimum compressive strength (44.3 MPa) and porosity (25.2%) were obtained when sintering was performed at 1350 °C for 1 h. Subsequently, ZTA_P/Fe composites without evident defects were fabricated by infiltration casting. Scanning electron microscopy, electron probe microanalysis and transmission electron microscopy were also used to analyze the microstructures and phase constituents of the interfacial layers of composites. Effects of applied wear loads on the wear behavior evolutions and wear mechanisms of composites were examined. Wear resistances of ZTA_P/Fe composites were found to be 1.64–2.21 times as compared to the Cr15 specimen.

(Y. Li et al., 2019) developed the interfacial bonding and wear behavior of iron matrix composites reinforced with ceramic particles. Using zirconia-strengthened alumina particles and Ni-Ti composite powder as raw materials, particle-strengthened high-Cr cast iron was manufactured by infiltration casting. 1mm diameter particles containing 80 vol.% ZrO2 were selected as reinforcement for high Cr cast iron matrix composites. Ni and Ti elemental powders (40–50 μm) were thoroughly mixed in ethanol using alumina grinding balls for 24 hours. Coated particles are formed by sintering in a graphite mold protected from an argon atmosphere. The sintering temperature was 1500°C, which is slightly higher than the melting point of Ni (1428°C), and the sintering holding time was 1 hour. The hardness of the Ni_3Ti, TiO and $AlNi_2Ti$ phases in the interfacial transition layer was measured by the nano-indentation method, which was 12.5 GPa, 16.1 GPa and 9.2 GPa, respectively. The three-body wear resistance of the composite reached 12.6 times that of high-Cr cast iron.

(Bhattacharyya et al., 2021) studied the fabrication routes along with the recent development in the area of iron based metal matrix nanocomposites. A detailed discussion was done on iron (Fe) metal matrix nanocomposites reinforced with aluminum oxide (Al_2O_3) prepared using powder metallurgy technique. Composites were prepared by sintering in an argon atmosphere in the temperature range of 900–1100 °C for 1–3 h. Hardness test was conducted on a Rockwell Hardness Tester using 1/8” H scale steel ball indenter. Specimens were tested for wear and corrosion using Pin on Disc wear and friction testing machine and gamry electrochemical cell. With the addition of aluminum oxide the hardness number reached up to 79 HRH and the wear rate was found out to be as low as 0.3 mm^3/Km. It was also revealed that with the addition of aluminum oxide, corrosion protection efficiency was 99.96% and cobalt doping further improved it to 99.99%.

The corrosion properties of iron-based composite materials containing graphite and silicon carbide (SiC) reinforcement were investigated. The effects of silicon carbide reinforcement were investigated by adding 0.5% graphite and 1%, 2%, and 4% SiC. A powder metallurgy method was used to produce the composite samples. Iron, graphite, and silicon carbide powders were blended for one hour with a three-axis mixer and then unidirectionally pressed under a pressure of 750 MPa. After pressing, the composite materials were sintered at 1100°C for one hour. The corrosion properties and microstructure, density, and hardness properties of the composite materials that can affect the corrosion properties were also investigated. It was determined that the pore ratio and hardness of the composite material increased, and corrosion resistance decreased, with increasing silicon carbide content (Karabulut et al., 2022).

The corrosion behavior and mechanism of a novel FeCrNi medium entropy alloy (MEA) prepared by powder metallurgy method in 3.5 wt% NaCl solution was investigated in the study. The results indicated that, compared with the 316L SS, the FeCrNi MEA exhibits outstanding corrosion resistance with a more positive breakdown potential (0.982 V_{SCE}) and lower current density ($8.317\times10{-}8A/cm2$) (Zhou et al., 2021).

2.5 MAX Phase (V_2AlC) Reinforcement

Sharma *et al*. (2021) studied the effect of Al content on the synthesis of V_2AlC ware investigated at 1400 °C and 1500 °C. The non-isothermal oxidation behavior of the V_2AlC MAX phase ware studied through Thermogravimetric Analysis (TGA) and the Differential Thermal Analysis (DTA) techniques. The thermal kinetics analysis is also performed during the oxidation of V_2AlC. The kinetic triplets such as activation energy, reaction mechanism and pre-exponential factors are determined. Moreover, thermodynamic calculations are performed to identify the reaction pathway involved during oxidation of the V_2AlC MAX phase. The results indicated that the nucleation mechanism dominated the oxidation process in the V_2AlC MAX phase.

Hossein-Zadeh *et al*. (2019) investigated the mechanical properties and microstructure of V_2AlC MAX phase prepared by the microwave sintering process. The powders mixture of the V-Al-C system with the molar ratio of 2:1.5:1 was mixed through a mixer mill for 10 min in the ethanol media without any aggressive milling condition. The microwave sintering process was performed at the sintering temperatures of 1200, 1300 and 1400 °C without any soaking times and the protective atmosphere in the graphite bed. The XRD patterns showed the formation of the V_2AlC max phase at the sintering temperature of 1200 °C with VC and Al_2O_3 compounds. In contrast, the sample sintered at 1300 °C displayed completely matched peaks with the reference pattern of the V_2AlC MAX phase.

Mohseni-Salehi *et al*. (2022) investigated the effect of different aluminum and vanadium precursors on the formation and physical properties of the V_2AlC MAX phase were studied. The results showed that the synthesis of V_2AlC is more favorable by elemental precursors than carbide precursors, and at least the presence of one metallic element is essential to accelerate the phase formation.

Liu *et al*. (2021) investigated high-purity ternary layered carbide V_2AlC powders have been prepared by a two-step modified molten salt method, i.e. by firstly synthesizing V_2C

with V and C powders at 900 °C, followed by preparing V_2AlC with V_2C and Al powders as reactants at 900–950 °C in molten (Na,K)Cl. The average particle distribution of V_2AlC powders was estimated to be ~400 nm. Molten salt as a reaction medium could promote the synthesis of V_2C and V_2AlC at lower temperatures. The synthesizing mechanisms of V_2C and V_2AlC in molten salts have also been discussed.

2.6 Manufacturing Thecnology for Metal Matrix Composite

MMCs can be made in a variety of ways. The process of production has a major impact on the final characteristics of MMC. With the appropriate modifications, MMC uses tried-and-true metal manufacturing processes. Choosing the optimal process depends on a number of factors, including the required MMC characteristics, cost, alloy matrix, distribution of reinforcing elements (particles or fibers), and product application. The techniques commonly used to create MMC can be broadly classified into two categories: liquid-process and solid-state techniques (Singh et al., 2022) The various fabrication techniques utilized to produce MMC are categorized as follows:

2.6.1 Liquid state processing

MMC production techniques known as "liquid-state processes" create composites by incorporating the reinforcing material into a molten metal matrix and then solidifying it. These processes are characterized by intimate interfacial bonding. This permits the formation of dense matrices and near-net-shaped components, even in complex geometries, at a remarkably quick rate of production. The one limitation of liquid-state processes is that high-temperature processing can result in the formation of a brittle interfacial layer between the involved phases, which has a negative impact on the composite properties. Uniform distribution of dispersed material without particles floating, sedimenting, or clustering/agglomerating in the molten alloy can be difficult (A. Kumar et al., 2021; Mussatto et al., 2021). Some types of these processes are discussed below.

Stir Casting: It is the method in which the reinforcement is mechanically stirred into a molten metal to achieve uniform distribution. After solidification, the casting is removed from the mold and subjected to various post-processing steps, such as heat treatment, machining, and surface finishing, to obtain the final desired properties and dimensions (Gotagunaki et al., 2023; Sankhla & Patel, 2022). The stir casting process has several disadvantages, including non-uniform reinforcement distribution, poor wettability, potential chemical reactions between the reinforcement and metal matrix, and reinforcement damage during the mechanical stirring process (Almadhoni & Khan, 2015; V. M. Kumar & Venkatesh, 2019).

In-situ processes: In-situ processing involves chemical reactions between the matrix and reinforcement. This reaction creates reinforcer phases in the form of precipitates. The reactive type process consists of two elements, which react exothermically to form the reinforcing phase. In the non-reactive type process, the monotectic and eutectic phases form the reinforcement and matrix during fabrication (Essien & Vaudreuil, 2022). The main advantage of this process is the ability to form a reinforcing phase in the matrix during the cooling and solidification processes. It also allows for uniform distribution, resulting in a strong bond between the matrix and the reinforcing phase. It has a controlled microstructure, reduced porosity, and high temperature performance (B. Das et al., 2016; Onal & Gavgali, 2017). The main disadvantage of the in-situ process is the limited selection of reinforcements that are thermodynamically stable within a particular matrix (Essien & Vaudreuil, 2022).

Infiltration: The composite production by infiltration method is carried out by impregnating a porous precursor material (such as ceramic particles, fibers, or woven) into molten metal to fill the pores. It can be defined as the method of sending fluid into the porous solid material by vacuum or gas. The driving force of the infiltration process can be capillary force or external pressure. The different types of infiltration methods are gas pressure infiltration, squeeze casting infiltration, and pressure die infiltration (Sree Manu et al., 2016).

2.6.2 Solid-Phase Process

A solid-state process is a method for creating metal matrix composites that uses high temperatures and pressures to create atomic diffusion between the metal matrix and the reinforcement. This process diminishes dispersed phase matrix wetting and reduces segregation effects and brittle reaction product formation. Additionally, high residual stresses during solidification are avoided, especially when compared to liquid-state processes. The materials that have a huge melting point difference are more easily fabricated through a solid-state process (Mussatto et al., 2021). Among the different types of solidphase processes, some of them are discussed below.

Friction Stir Processing (FSP): It is an environmentally friendly surface composite fabrication and surface modification process that uses the same principle of friction stir welding (FSW). This technique is gaining popularity as a promising way to create surface metal matrix composites (Parray et al., 2021).

Laser Cladding: Laser cladding is a modern manufacturing technique for altering the surface of metallic materials in today's industries. This method includes the deposition of a new layer on a substrate by laser fusion of blown powders or pre-placed powder coatings. It is used to increase the surface qualities, such as wear resistance, hardness, oxidation resistance, corrosion resistance, biocompatibility, and heat resistance, by depositing a thick layer of modern materials on their surface (A. K. Das, 2022).

Powder Metallurgy Process: This technique is the most common solid-state process that is suitable for the fabrication of micro- and nano-ceramic-reinforced MMCs. PM routes are extensively used for investigations of new composites and for the production of MMCs (Mussatto et al., 2021).

2.7 Powder Metallurgy Technique

PM is used to produce a net-shape/near-net-shape molding process with a wide range of properties that are used to synthesize denser, more precise, and more robust MMC components (Meignanamoorthy & Ravichandran, 2018). Powder metallurgy is a technology that mixes fine powders such as metals and ceramics, forms them into the desired shape, and heats and bonds (sinters) the compressed materials in a controlled atmosphere. This is one of the best ways to compact powder composites in a mold to achieve desirable properties such as reduced porosity and a more uniform distribution of reinforcement, as well as adequate compaction of the ground powder (N. Kumar et al., 2021).

Powder metallurgy uses powders of metals or alloys as raw materials to produce highly accurate finished parts at competitive costs, saving energy and time. Sintering in air maintains a temperature below the melting point throughout the process (Khazaal et al., 2022).

It consists of the following steps:

2.7.1 Powder preparation and mixing

In the powder metallurgy technique, mixing powders is imperative to achieving the desired material properties. The primary objective of mixing is to achieve a uniform distribution of the reinforcement particles within the matrix metal powder. Mixing factors such as mixing time, mixing intensity, and the use of binders or lubricants can affect the uniform powder distribution and the resulting microstructure of the final product. The mixing quality has a significant impact on the final properties of the material, with factors like particle size, mixing time, and uniform dispersion having key roles. The mixing/milling time should be long enough to obtain a more uniform mixture by reducing the agglomeration or clustering of particles, but overmixing can decrease particle size, alter particle shape, and work harden particles. Moreover, controlling the atmosphere during mixing helps to avoid contamination, such as the formation of oxides on particle surfaces (Edosa et al., 2022; N. Kumar, Bharti, & Saxena, 2020).

2.7.2 Compaction

The powder compacting process in the powder metallurgy technique is important to achieve high product density and uniformity of that density throughout the compact. This process involves compressing powder into a shape known as a green compact. Higher compacting pressure is used to increase green density, which is essential for achieving high product density and uniformity throughout the compact. Parameters such as compaction pressure, compaction speed, and dwell time influence the density, dimensional accuracy, and mechanical properties of the green compact (N. Kumar, Bharti, Dixit, et al., 2020).

A lubricant, such as graphite, molybdenum sulphide ought to be used between the die wall and the powder to allow for die compression. This is because the friction between the powder and die wall during die compression results in an uneven density distribution, which leaves the green body with residual stresses. When the PM pieces are subsequently subjected to high temperature consolidation, this could result in undesirable flaws like pores and cracks, (Honnaiah et al., 2023).

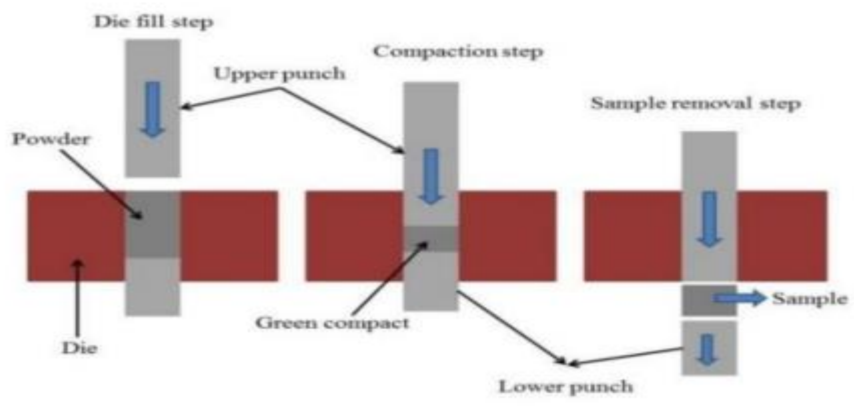

Figure 2.3 Compaction Process (Panda, 2016).

2.7.3 Sintering

The sintering process is a heat treatment applied to green compact at a high temperature below the melting point of the major constituent of the powder metallurgy material in a controlled atmosphere. It is used to increase the bond between particles and enhance the strength of the powder metal compact, leading to the desired properties in the final product (Edosa et al., 2022). Sintering parameters like temperature, heating rate, holding time, and atmosphere influence densification, grain growth, and the final mechanical properties of the sintered part. Post-sintering processes such as heat treatment, machining, surface finishing, and coating can further modify the properties and surface characteristics of the sintered part (Behera et al., 2019).

2.8 Multi-Response Optimization Method

The Multi-Response Optimization Method is a technique used to optimize multiple results simultaneously. In engineering, multi-response optimization is essential to obtaining the best overall system performance by considering and balancing various factors simultaneously. This method enables engineers to find solutions that enhance all responses without compromising any particular response. The responses in multi-response optimization may not compete with each other, and the goal is to optimize all responses simultaneously to improve overall product or system performance (Beshah et al., 2015; Winarni & Indratno, 2018)(Beshah et al., 2015).

The main methods used for multi-response optimization are the Taguchi Method, Grey Relational Analysis (GRA), and Data Envelopment Analysis (DEA) (Y. Kumar & Singh, 2014; Mardani et al., 2017). GRA is a method that can be used in conjunction with the Taguchi method, allowing it to take advantage of the benefits of both methods to solve multiresponse optimization problems. It aims to measure the similarity or closeness between different response profiles and identify the input variable settings that maximize the overall closeness or similarity to the desired response. This method is a more suitable technique, and it is easy to predict the effects of different parameters within the levels studied. In the GRA method, the parameters obtained from the Taguchi method are converted to a single performance characteristic called the grey relational grade for the optimization of multiple performance characteristics. Grey relational analysis is particularly useful when dealing with complex systems, limited data, or uncertain environments. It allows for a comprehensive assessment of multiple responses and facilitates decision-making by identifying the input variable settings that lead to the best overall performance or closeness to the desired targets (Girish et al., 2019; Hussain et al., 2020).

2.9 Literature Summary

The surveyed literature show that Iron based metal matrix composites have been reinforced with various ceramic materials, such as, Al_2O_3, ZrO_2 and multi-walled carbon nanotubes material. By adjusting the weight composition of the reinforcements and modifying different process parameters, both mechanical and tribological properties of the base material were observed to change. These studies demonstrated that ceramic additives are materials that possess excellent bonding capabilities, effectively enhances the strength of the Iron based matrix materials. Further research can be undertaken to investigate the impact of reinforcement composition, fabrication techniques, and input process parameters on the mechanical and tribological properties of Iron based metal matrix composites.

2.10 Research Gap

Some studies have been conducted on iron based metal matrix composites, which are known for their high strength, hardness and wear resistance. However, the challenges encountered with the mild steel alloys in various applications are low specific weight to strength ratio, less wear resistance and corrosion resistance because mild steel consists of a low amount of carbon, typically between 0.05% and 0.25%, its easily corroded when exposed to moisture and its high density (7.85 g/cm3). Existing literature has extensively explored on synthesis, testing characterization of iron reinforced with some powdered reinforcement. Notably, there is no yet documented research has been carried out on reinforcing of iron with vanadium aluminum carbide max phase powder particles. This study aimed to address the gap by reinforcing iron with V_2AlC max phase for various applications particularly in aerospace and automobile and marine applications where specific weights to strength ratio, hardness, wear resistance and corrosion resistance are of major concern. Additionally, this work will employ optimization technique to determine the optimum input process parameter using Taguchi based grey relational analysis.

CHAPTER THREE: MATERIALS AND METHODS

3.1 Introduction

This chapter covered the materials used to create iron-based metal matrix composites, sample preparation techniques, experimental procedures, and testing setups, as well as the tools and instruments used and data analysis techniques. Pure Iron powder as matrix and reinforcement V_2AlC and Graphene Oxide was used. The selection was based on cost, properties, and availability.

3.2 Materials and Equipment's

To ensure the appropriate selection of matrix and reinforcement materials for the intended research, it is crucial to possess a comprehensive understanding of the properties and applications of both the matrix and reinforcing materials. It is important to understand the necessary properties of the material used in aerospace, automobile, marine and other industrial application. All properties used in the analysis of the mechanical, tribological and microstructural properties and other properties of the material were listed.

3.2.1. Pure iron metal

Iron is the main component of ferrous metals, alloys, and steels. To create cast iron or steel, iron is alloyed with carbon, nickel, chromium, and other elements. In this research commercially available iron powder with purity of 99.8% was considered as the matrix for the fabrication of the composite material.

Table 3.1 Chemical composition of iron with different elements (Satyendra, 2016)

Element	%	Element	%
Carbon	0.004	Silicon	0.001
Manganese	0.04	Phosphorous	0.004
Sulphur	0.007	Aluminum	0.001
Arsenic	0.002	Boron	0.001
Nitrogen	0.006	Niobium	0.001
Tin	0.001	Titanium	0.001
Vanadium	0.001	Lead	0.002
Bismuth	0.001	Calcium	0.0002
Tellurium	0.001	Hydrogen	1.1ppm

Iron powder was chosen since it is more workable, stronger, and suitable for a number of uses in the construction and automotive industries in order to function better in metal matrices by creating heat. pure iron powder was purchased from Parshwamani metals manufacturer, India with an average particle size of (50-150μm), density 7.874 g/cm3 at 25 ºC, and 99.8% purity) used as matrix.

Table 3.2 Mechanical and physical properties of pure iron (www.azom.com)

Mechanical Properties	Metric	English
strength at break	540 MPa	78300 psi
Yield strength	50 MPa	7250 psi
Poisson's ratio	0.291	0.291
Modulus of elasticity	200 GPa	29000 ksi
Shear modulus	77.5 GPa	11200 ksi
Hardness, Vickers	150	150
Density	7.87 g/cm^3	0.284 lb/in^3
Melting point	1536 °C	2797°F
Boiling point	2861 °C	5182°F

3.2.2 Vanadium aluminum carbide powder

V_2AlC is a ternary nano-laminated hexagonal compound that belongs to the family of MAX phases. The general formula of the family is $M_{n+1}AX_n$, where M refers to the transition metal, A is metal and X is carbon or nitrogen (P. Sharma et al., 2021). V_2AlC materials possess spectacular performances associated with either ceramics or metals, such as excellent machinability, good electrical and thermal conductivity, low friction coefficient as well as superior resistance to oxidation and corrosion of these MAX phases .

Table 3.3 Physical properties of V_2AlC (P. Sharma et al., 2021)

Properties	Metric
Molecular weight	140.87
Melting point	2000 °C
Density	4.85 g/cm^3

3.2.3 Graphene oxide

Graphene oxide (GO), also referred to as graphite/graphitic oxide, is produced by treating graphite with oxidizers, and results in a compound of carbon, oxygen, and hydrogen in variable ratios. The structure and properties of GO is much dependent on the particular synthesis method and degree of oxidation. GO swells and absorbs moisture proportionally to humidity in liquid water. GO membranes are vacuum-tight and permeable to water vapors, but impermeable to nitrogen and oxygen. The ability to absorb water by GO depends on the specific synthesis method and also shows a strong temperature dependence.

3.2.4 Equipment's

Different testing and manufacturing equipment were also utilized throughout the experiments during measuring and testing the specimen. It is listed in Table 3.4 below with their specific tasks during the manufacturing of MMMC samples.

Table 3.4 The equipment used in Testing and Manufacturing processes

No.	Equipment's	Functions
1	Electronic weighing machine	To measure the weight percentage of matrix and reinforcement and weight loss during the wear test
2	Ball milling	For crashing and mixing
3	Hydraulic pressing machine	Used to compact the composite materials powders
4	High-temperature box Furnace	For sintering the green compact at various temperatures with a specific heat rate.
5	Grinding and polishing	To make a scratch-free, flat surface of the specimen by removing the damages
6	Optical Microscope (OM)	To investigate the surfaces morphology
7	Vickers hardness machine	To examine the hardness property of the samples
8	Universal testing machine (UTM)	To test the resistance of the compressive load applied to the specimens
9	Pin-on-disc	To test the wear behavior of the optimal specimen.

3.3 Methods

In this work, a powder metallurgical process was used to prepare iron matrix composite samples reinforced with V_2AlC/GO. The stages for mixing, compacting, sintering, manufacturing, and testing are shown in the accompanying figure. A typical flow map of ongoing research activity is shown in Figure 3.1.

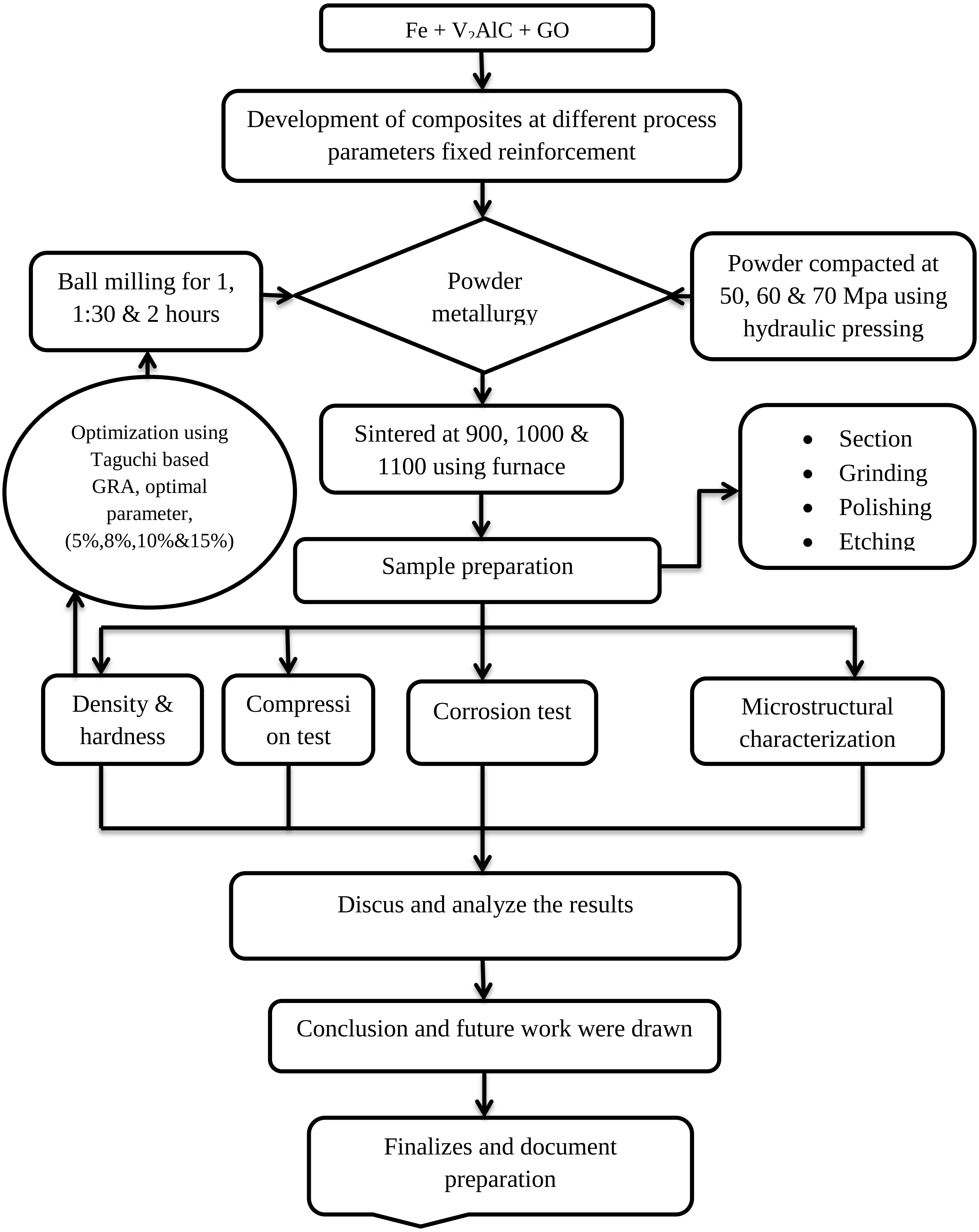

Figure 3.1 Flow chart for experimental procedure

3.3.1Design the experiment for IMMC fabrication

Based on surveys of the literature, thirteen samples were chosen to create the new Fe-based MMC samples. From those samples, nine samples that had been synthesized in the first experiment at constant weight reinforcement ratio with different powder metallurgy process parameters, developed by L9 orthogonal array by considering three factors and three levels and the rest four samples had been manufactured with optimal process parameters for varied weight ratio in the second experiment as shown in Table 3.5. The powder metallurgy method was used to build the composites, which were made in advance based on the main input process parameters (milling time, compaction pressure, sintering temperature, and weight fraction of reinforcement).

Table 3.5 Reinforced IMMC manufactured through powder metallurgy

No.	Fe %	V_2AlC %	GO %	MT (hrs.)	CP (MPa)	ST (^oC)
S_1	91	5	4	1	50	900
S_2	91	5	4	1:5	70	900
S_3	91	5	4	2	60	900
S_4	91	5	4	1	70	1100
S_5	91	5	4	1:5	60	1100
S_6	91	5	4	2	50	1100
S_7	91	5	4	1	60	1000
S_8	91	5	4	1:5	50	1000
S_9	91	5	4	2	70	1000

Whereas, for the rest four samples were manufactured with optimal process parameters, based on previously manufactured and tested samples, that one had better properties.

Table 3.6 Reinforced IMMC manufactured through powder metallurgy at optimal level

Sample's	Materials (in weight %)			Process parameters		
	Fe	V_2AlC	GO	MT(A)	CP(B)	ST(C)
S_{10}	91 %	5 %	4 %	1	70	1000
S_{11}	88 %	8 %	4 %	1	70	1000
S_{12}	86 %	10 %	4 %	1	70	1000
S_{13}	81 %	15 %	4 %	1	70	1000

3.3.2 Powder metallurgy fabrication techniques

Powder metallurgy technique was used to fabricate quality MMC products with more near net shaped object with utmost dimensional accuracy (Gupta et al., 2015). PM is one the most economical process for fabricating the near net particulate reinforced MMCs and thereby allowing greater flexibility, a significant reduction in manufacturing costs due to minimizing machining process and minimized scrap losses.

In this research work, the main goal of the selection of powder metallurgy was to develop hybrid metal matrix composites with the best mechanical properties to fabricate tool material with high corrosion resistance and wear resistance. The steps involved in the powder metallurgy technique are listed below. Samples fabricating through powder metallurgy process can be divided into three basic sequence steps:

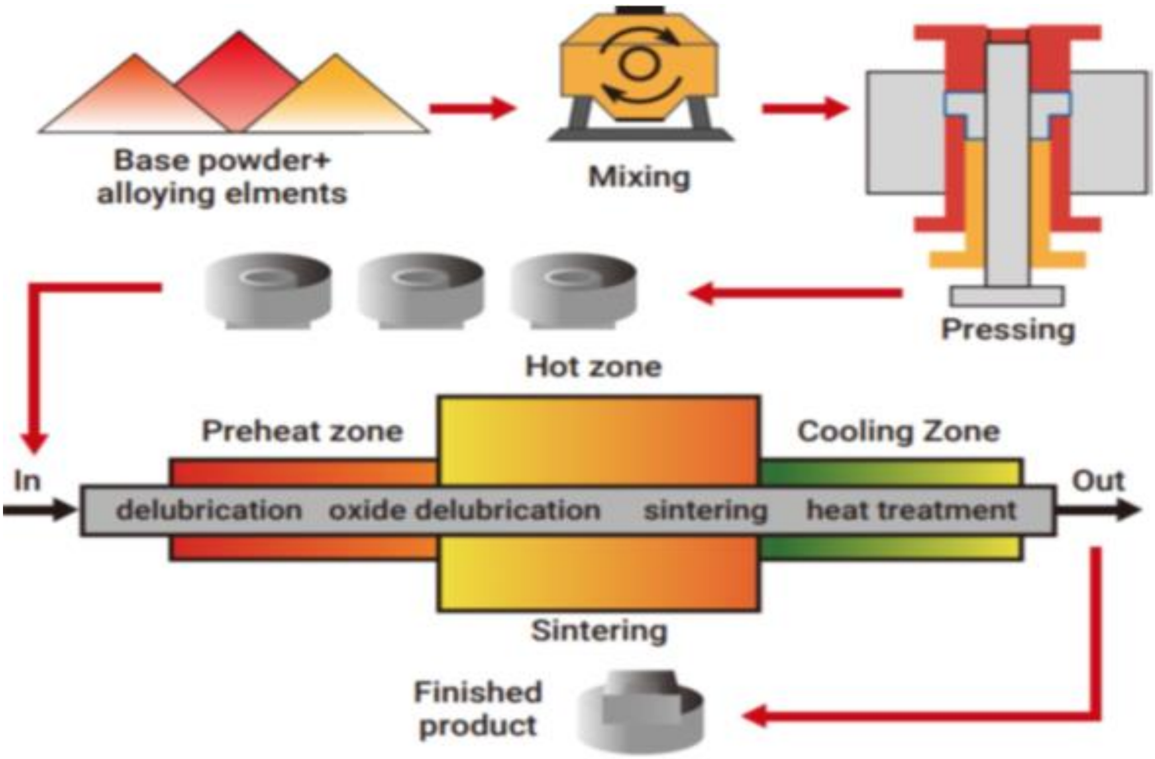

Figure 3.2 Schematic of powder metallurgy process (Singh et al., 2023)

Powder mixing

In order to achieve the desired performance of the selected powders in the manufacturing of composites, mixing refers to the homogeneous blending of different types of powders, and it is essential to distribute them evenly throughout the matrix. This has been accomplished through the use of high energy ball milling machines. Zirconia balls were used to ball mill metal alloy powders in a high velocity chamber. In order to ensure the end product's structural and physical integrity, high-energy ball mills are also used to produce fine particles from alloy powders.

(a) (b)

Figure 3.3 (a) High Energy mixer/mill machine (b) Zirconium balls

In this study, 5% of V_2AlC and 4% GO powder were mixed with 91% of pure iron in sample one for fabricated nine samples (three trial samples for each) with different powder metallurgy process parameters for first round and then 5%, 8%, 10% and 15% of V_2AlC were mixed with 88%, 86% & 81% of pure iron respectively at constant 4% of GO for the rest four samples at optimal PM process parameters. A high energy planetary ball mill was used to mix the powder by using zirconia balls (Jha et al., 2022). The milling conditions adopted in the present research work are:

Milling Parameters:

- ✓ Milling speed: 200 rpm
- ✓ Milling time: 1, 1:5 and 2 hours
- ✓ Ball diameter: 10mm
- ✓ Ball to powder weight ratio: 10:1
- ✓ Temperature of milling (at room temperature).

Powder compaction

Powder compaction is the process of compressing the Fe-V_2AlC-GO mixed powder in a mold using a hydraulic mounting press. The combined powder was accurately measured with a weighted balance. The powder mixture was pressed into a cylindrical shape (d=12mm, h=20mm) using a carbon steel die using a hydraulic press with a load of 120 KN. Cold pressing was performed at a pressure of 50, 60 &70 MPa (Olani et al., 2023) and a holding time of 10 minutes. Typically, the tool is held vertically and the punch tool forms the bottom of the cavity. The compressed samples are then ejected from the mold cavity. The density of compacted powders is directly proportional to the pressure applied.

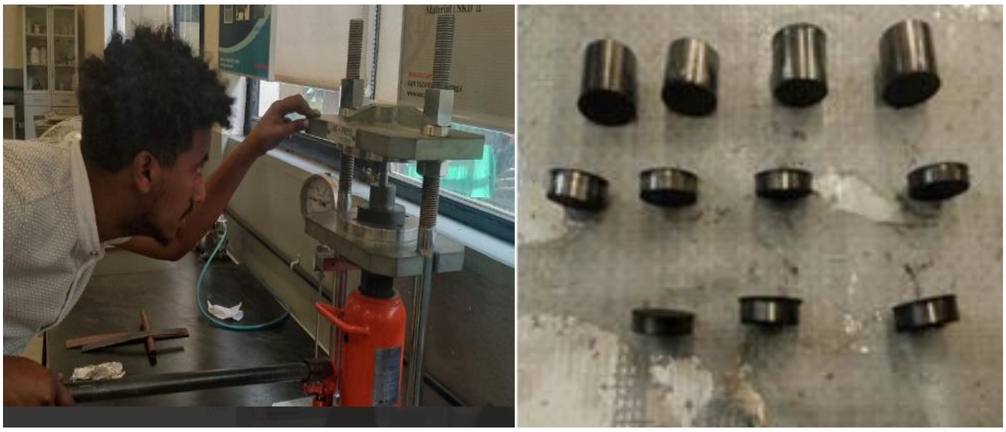

(a) (b)

Figure 3.4 (a) Mounting Press set up and (b) Compacted Specimen (Green Part)

Sintering

The green compressed sample's does not have sufficient strength and the particles are loosely bound together and may crash easily at low loads. It may also contain inter particle voids. Sintering is performed after compaction to reduce porosity and create metallic bonds between powder particles (R. Das et al., 2022). After deformation, particle formation and growth, and cooling, the powders combine to form solid pieces. During sintering, bonding occurs between agglomerated powder particles (Issa et al., 2023; D. K. Sharma et al., 2020).

(a) (b) (c)

Figure 3.5 (a), the furnace setup and (b) green compact and (c) the sintered samples

3.4 Specimen Preparation for Testing and Microstructural Characterization

After the manufacturing of composite materials by powder metallurgy at optimal parameters, composite green sintered samples were prepared for microstructural characterization, physical, mechanical, wear, and corrosion testing. Samples were prepared by grinding, polishing, etching, hand sawing, and file to remove excess material and minimize dimensions to obtain the required sample geometry and dimensions for various tests according to ASTM standards.

The main steps for sample preparation (optical microscopy, X-ray diffraction) are: Cutting (sectioning), grinding (rough and fine grinding), polishing, etching, and then microscopic inspection.

Sectioning

A cross-section of the sample to be tested was created by cutting the prepared sample. Use a hand saw and file to reduce the size of the sample to be placed on the stage of the light microscope, as shown in the figure 3.8 (A).

Grinding and polishing

The sintered Fe-V_2AlC-GO composite samples were progressively finely ground using emery paper and ground with a grinder for hardness testing and microstructural analysis. The purpose of grinding and polishing is to obtain a flat, mirror-like surface without excessive distortion. This achieved in three steps, rough sharpening, fine sharpening, and polishing. Polishing is the process of rendering the Fe-V_2AlC-GO composite samples scratch-free using sandpapers of progressively increasing grit from 240, 800, 1200, and 2000 as shown in figure (C), It was then exposed to grinding using sand papers from coarse to fine grades with orientation of 90 degree 42 from the previous direction of grinding, as shown in Figure (B). Polishing is the process of rubbing the sample with a diamond suspension to create a smooth, shiny surface while gradually reducing the pressure and rotation speed of the sanding disc in the RB 204 Metpol II model polishing process, as shown in the figure below (D).

Etching

Polished samples of both matrix and composite were etched with the recommended nital solution of 4% nitric acid and alcohol mixed etchant, which was performed by simply immersing the sample in the prepared etchant for 30 seconds, as shown in figure (E). The samples are then washed with distilled water before the microstructural characterization.

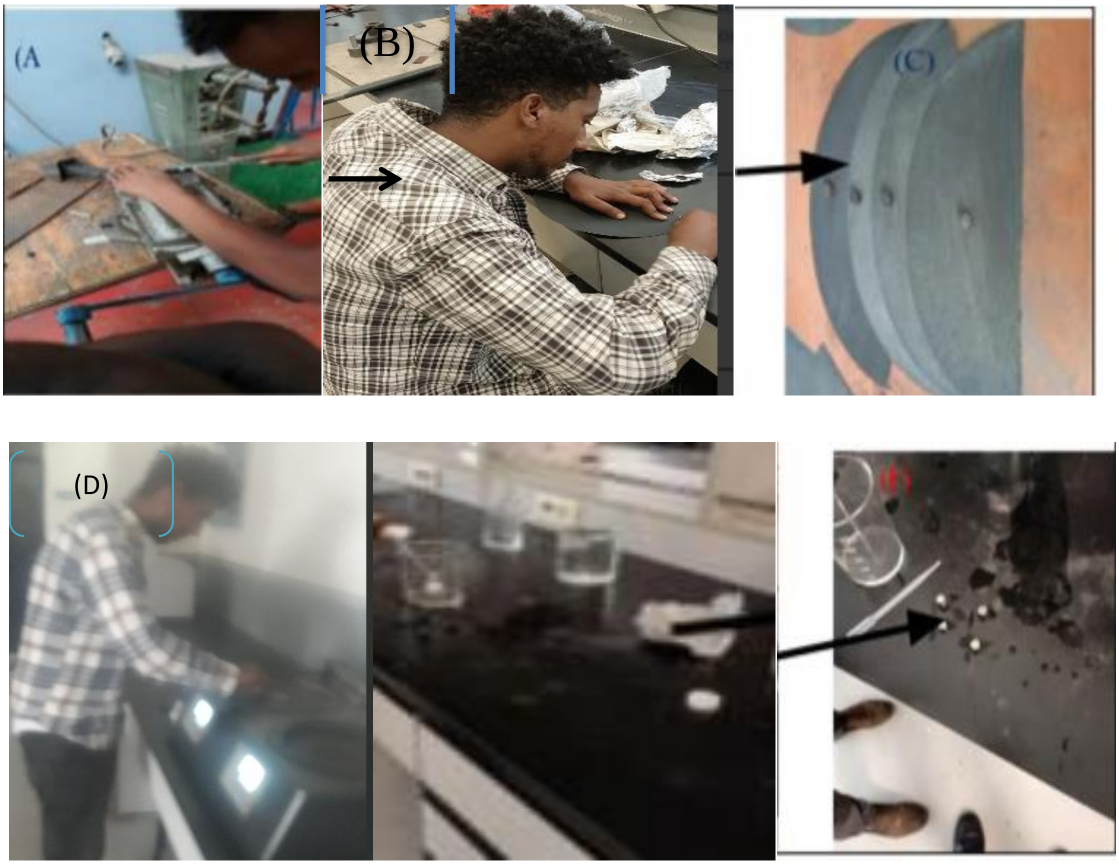

Figure 3.6 Samples preparation for characterization

3.5 Experimental Procedure

After the manufacturing of composite materials those fabricated through different powder metallurgy process parameters (milling time, compaction pressure and sintering temperature) physical and mechanical properties were tested.

3.5.1 Density of composite materials

In this stage density were tested for developed nine samples (three trial for each) based on powder metallurgy process parameters. Density is a physical property of a material that describes its mass per unit volume. It is an important property of materials, particularly in engineering applications where weight and strength are critical factors. The composition and structure of the MMCs, as well as the manufacturing method used to produce them, can affect density. In this research, the density of the specimens was measured using the Archimedes method to identify the effects of powder metallurgy process parameters and reinforcements. The procedure of this method involves: first measuring the mass of the composite specimen in air ($Wair$), then immersing the specimen in a liquid medium, typically water, and measuring the mass of the sample while submerged ($Wair$). Finally, the density of the composite specimen was calculated using equation. As per ASTM B962-23, the surface roughness of the specimens was removed using 120-grit sanding, and surface pores were sealed by oil impregnation. The relation for calculating the density of the specimen by Archimedes method is as follows:

$$\rho_{sample} = \frac{W_{Air} \times \rho_{Fluid}}{W_{Air} - W_{Fluid}} \quad (3.1)$$

Where: ρ_{sample} = Sample density

W_{Air} = Sample weight in the atmospheric air

W_{Fluid} = Sample weight in the fluid

ρ_{Fluid} = Fluid/Water density (0.9982 g/mL at 20 °C)

3.5.2 Porosity of composite materials

Porosity is the existence of space or pores in the structure of composite materials. It represents the fraction of overall volume of the composite that is occupied by these void spaces. The porosity is denoted by the symbol ϕ, and its value ranges between 0% and 100% when it is expressed as a percentage or between 0 and 1 when it is expressed as a fraction. In MMCs, the presence of voids or pores can significantly affect the material's properties, including its strength, stiffness, and hardness. The two commonly used techniques to determine porosity in metal matrix composites (MMCs) are: Archimedes' Method and Image Analysis. But this study employed Archimedes' method, which is based on the principle of buoyancy and is widely used for porosity determination in MMCs. This method provides a direct measurement of the overall porosity in the composite.

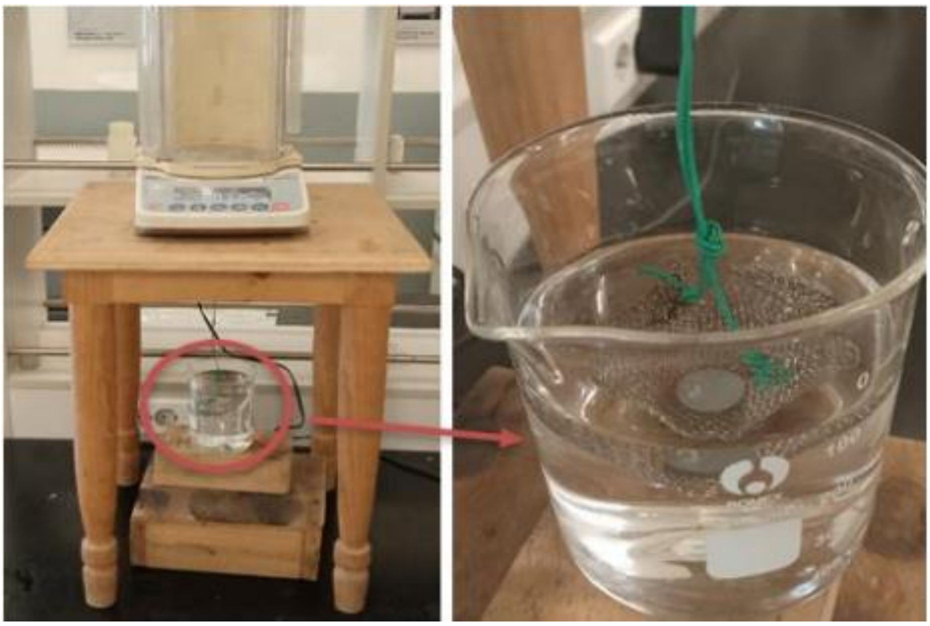

Figure 3.7 Archimedes methods of density measurement in distilled water

The steps involved in the Archimedes’ method are as follow:

a. Calculate the volume of the specimen using the density of the liquid, typically water.

$$\text{Buoyant force} = W_{Air} - W_{Fluid} \quad (3.2)$$

Volume of specimen = Buoyant force / Density of liquid (ρ_{Fluid})

$$V_{Sample} = \frac{W_{Air} - W_{Fluid}}{\rho_{Fluid}} \quad (3.3)$$

b. Calculate the apparent density of the composite using the weight in air and the volume.

$$\text{Apparent density } (\rho_A) = \frac{W_{Air}}{V_{Sample}} \quad (3.4)$$

c. Calculate the theoretical density of the composite, which can be calculated based on the composition of the matrix and reinforcement materials.

$$\rho_t = (\omega_m \times \rho_m) + (\omega_r \times \rho_r) \quad (3.5)$$

Where: ρ_t = theoretical density

Ш_m = weight fraction of the matrix material

ρ_m = density of the matrix material

Ш_r = weight fraction of the reinforcement material

ρ_r = density of the reinforcement material

d. Finally, calculate the porosity using the formula:

$$\text{Porosity } (\phi) = \frac{\text{Theoretical density} - \text{Aparent density}}{\text{Theoretical density}} \times 100$$

$$\phi = \frac{\rho_t - \rho_A}{\rho_t} \times 100 \qquad (3.6)$$

3.5.3 Hardness test

Hardness is the ability of a material to resist deformation, indentation, or scratching. It is a very important test in engineering applications as it shows a material's ability to withstand wear, friction, and erosion by external factors. The various hardness testing methods available are the Brinell Hardness Test, Rockwell Hardness Test, Vickers Hardness Test, Knoop Hardness Test, and Shore Hardness Test. Among them, in this research, the Vickers hardness test method was used. This method is based on the indentation of a specimen's surface using a diamond indenter in the shape of a square-based 136° pyramid. The test involves applying a specific load to the specimen's surface using a Vickers hardness testing machine (brand name: HVS-50).

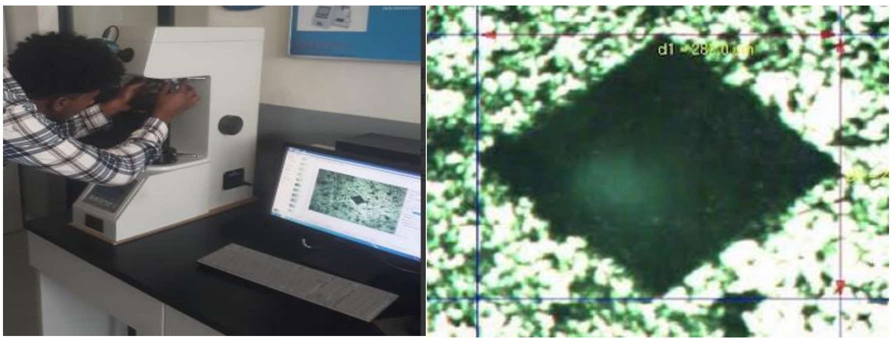

Figure 3.8 Vickers Hardness Test and Measurement

As shown in Figure 3.7, apply a uniform load without impact and push the indenter into the specimen. The load used for hardness test was10 kgf with 5 seconds a holding time. The indentation size was measured using a microscope or an automated measurement system.

The two diagonals of the indentation were measured, and their average length was used to calculate the Vickers hardness number (HV) using equation (3.7). This test was conducted as per ASTM-B933-16 for all specimens.

The Vickers hardness number is calculated using the formula:

$$HV = \frac{\text{Constant} \times \text{Test force}}{\text{Surface area of indentation}}$$

$$HV = \frac{0.102 \times 2F(\sin \frac{136^{\circ}}{2})}{d^2} \tag{3.7}$$

Where: HV = Vickers Hardness number

F = applied load in kilograms-force (kgf)

d = average length of the diagonals of the indentation in millimeters (mm)

3.6 Data Analysis and Optimization Method

In this study data analysis and optimization are crucial to identify the point at which milling time, compacting pressure, and sintering temperature are effective. The process parameters (such as milling time, compacting pressure and sintering temperature) were analyzed through Taguchi-based GRA optimization technique, based on the experimental results obtained from physical tests and mechanical tests. In this study, the response data were examined using multi-objective optimization technique i.e. GRA to obtain the optimal level combination of the process parameter for the factor. GRA based Taguchi method is appropriate for data analysis to provide an optimum sample during the analysis of interrelationships between multiple responses using the response graph method. The steps used to implement grey relational analysis are shown below. At first, the response data were converted to S/N ratios (η or Yij) based on Taguchi Quality Loss Function (QLF) to minimize the sensitivity of quality characteristics to noise factors. Type of quality characteristics are smaller the better, nominal the best, and larger the better (Rajyalakshmi & Venkata Ramaiah, 2013; P. K. Sahu & Pal, 2015).

Step 1: Change the replicated response data into the S/N (η) ratio (Xi) using the following formulas:

For the smaller better,

$$\eta = -10 \log \left[\frac{1}{n} \sum_{i=1}^{n} {X_{ij}}^2 \right] \quad (3.8)$$

For the larger better,

$$\eta = -10 \log \left[\frac{1}{n} \sum_{i=1}^{n} \frac{1}{{X_{ij}}^2} \right] \quad (3.9)$$

Where: η = Signal to noise ratio, X_{ij} = experimental value per trial, n = number of replication, and i = number of trial.

Step 2: Normalize the data in order to eliminate the influence of different measurement units and to ensure that all the data sets are transformed into comparable ranges. After this process, the data values obtained range between 0 and 1. . Since the objective of this study is to minimize the density and increase strength and hardness, the smaller the better and larger the better for hardness and density were taken for analyzing the quality respectively, the equation of larger the better were used as stated below (P. K. Sahu & Pal, 2015).

$$Y_{ij} = \frac{X_{ij} - \min(X_{ij})}{\max(X_{ij}) - \min(X_{ij})} \quad (3.10)$$

And, the formula of the smaller the better for porosity normalization method is,

$$Y_{ij} = \frac{\max(X_{ij}) - X_{ij}}{\max(X_{ij}) - \min(X_{ij})} \quad (3.11)$$

Where: Y_{ij} = normalized value for ith trial for jth response, X_{ij} = S/N ratio value for ith trial for jth response, i = trial number (i = 1, 2, …, n) and j = response number (j = 1, 2, …, m).

Step 3: Compute the coefficient of grey relational for the normalized values (Kuo et al., 2008; P. K. Sahu & Pal, 2015).

$$\delta_{ij} = \frac{\triangle_{min} + \Upsilon \triangle_{max}}{\triangle_{ij} + \Upsilon \triangle_{max}} \quad (3.12)$$

Where: δ_{ij} = grey relational coefficient for the ith trial and jth, △ = deviation sequence of reference value ith and jth normalized value of the responses, $\triangle_{max}$ & $\triangle_{min}$ denotes the maximum and minimum values of "Δ" respectively, Υ = maximum value of normalized S/N ratio distinguishing coefficient which is defined in the range $0 \leq \gamma \leq 1$.

Step 4: Calculate the grey relational grade (βi). At the last, the grey relational grades were calculated using Eq. (3.13) for selecting optimal levels for the process parameter. Optimal level for factors as well as influential process parameter was analyzed further using the response graph method.

$$\beta_i = \frac{1}{m}\sum \delta_{ij} \tag{3.13}$$

Where: m = number of responses

3.7 Test and Characterization of Optimized Parameter Samples

In this study two experiment were investigated, the first experiment was examined the samples fabricated with different powder metallurgy process parameters, at fixed reinforcement (5% of V_2AlC with 4% of GO as lubricant) for all nine samples and next experiment was conducted for samples fabricated based on optimal process parameters, four samples fabricated and examined with varying reinforcement (5%, 8%, 10% & 15% of V_2AlC with 4% GO) to investigate the effect of reinforcement on optimal level and additional pure iron sample for comparison. Physical (density and porosity) and mechanical (hardness) test were examined based on the previous procedure.

3.7.1 Compression strength test

Compressive strength of a material is the ability of the material to withstand compressive loading without failure. Compression testing is used to evaluate the compressive strength and mechanical properties. In this study, a compression test was performed using a Universal Testing Machine (UTM) (model: UTN/E-100) as per the ASTM B925–15 standards. This test was conducted by applying the compressive load gradually to the specimen until it failed. The UTM used has a data acquisition system, so test results were analyzed automatically and reported on the screen of the computer-aided UTM.

Figure 3.9 The Universal Testing Machine (UTM) for compression test

Compressive strength was determined by gradually applying a load to an iron metal matrix composite sample calculated using the applied compressive load, force per cross-sectional area of the sample.

$$\text{Ultimate compressive strength (USC)} = \frac{F}{A} \quad (3.14)$$

3.7.2 Corrosion test

Corrosion is the gradual deterioration of materials (usually metals) through chemical or electrochemical reaction with their environment. Corrosion tests were performed by immersing the specimens in a 3% NaCl bath for 30 minutes. The specimens for the testing were 12mm in diameter and 8mm in length. Composite specimens were polished with emery polishing paper 800, 1200, and finally with 12 m diamond paste on a double disc polishing machine to remove any accidental marks from the surface of the specimen and make it mirror like surface. An electrochemical analyzer (SP300 EC-LAB, Biologic Science Instruments, ASTU, Material science laboratory) were used to perform the electrochemical measurements in a three-electrode cell.

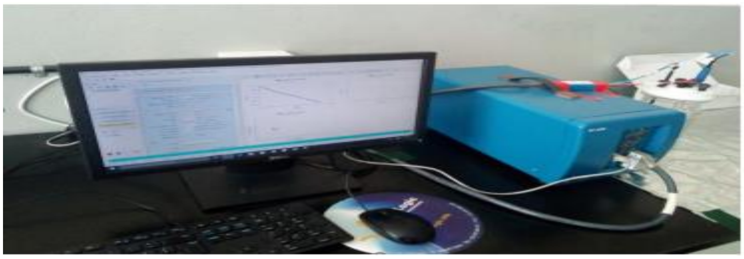

Figure 3.10 Electrochemical Analyzer

The Tafel curve describes the relationship between current density and overpotential in electrochemical reactions. It provides information about the corrosion potential (Ecorr) and corrosion current (Icorr), which can be used to assess the corrosion behavior and resistance of the material. Corrosion potential refers to the electrode potential at which anodic and cathodic currents are equal and no net current flows. This potential is an important parameter to determine the corrosion behavior of material. Because the greater the corrosion potential, the lower the likelihood of corrosion. The corrosion current is the current density at the corrosion potential, and it is an important parameter that quantifies the rate of electrochemical reactions occurring on the surface of a corroding material. The lower corrosion current density indicates a slower corrosion rate. The corrosion rate of the optimum composite was computed using the following Stern-Geary equation (Zainuri & Bäßler, 2019).

$$\text{Corossion rate (mmpy)} = 0.00327 \times \mathrm{I_{corr}} \times \frac{\mathrm{E_w}}{\mathrm{d}} \quad (3.15)$$

Where: $\mathrm{I_{corr}}$ = corrosion current, $\mathrm{E_w}$ = equivalent weight (g), d = density (g/cm^3)

3.8 Microstructural Characterization of Sintered Samples

In order to investigate the mechanical properties (hardness and compressive strength), and microstructural properties of optimized Fe-V_2AlC-GO composites, experimental test procedures measuring density and porosity values were performed. The purpose of microstructural testing is to characterize the microstructural properties of metals, such as: Grain size, segregation, distribution of different phases, types of constituent phase occurrences, and non-metallic inclusions such as slag and sulfides. As part of this study, X-RD and OM were performed for the above properties.

3.8.1 X-Ray Diffraction (XRD)

(A) Phases analysis in sintered composite

Using an X-ray diffractometer (XRD) with an XRD-7000 X-ray diffractometer Maxima model from Shimadzu Corporation (Japan), crystalline phases and elements of IMMC samples using respective sample preparation methods and sample holder devices. Phase analysis of the sintered samples was performed by X-ray diffraction (XRD, at ASTU) observation with Cu-Kα radiation at 40 kV and 30 (mA) at 2θ value in between (80°-100°) in 3° /min scan rate. Phase identification and quantitative phase analysis were performed by using origin pro-2022. The crystalline phase of the matrix and reinforcement's present in the sintered composite was analyzed.

(B) Determination of crystalline size and lattice strain by XRD peak analysis

Gauss method of X-RD peak profile analysis was employed to calculate the microstructural parameters namely crystalline size, mean squared lattice strain, root mean squared strain, and dislocation density (Venkateswarlu et al., 2014) of Fe-V_2AlC-GO by using XRD data. According to an analysis of X-ray peak broadening, the sample's elemental composition and its preparation conditions affect the X-ray diffraction lines' intensity. The atomic fine structure of prepared sample's analyzed by correlating the observed X-ray diffraction peaks to atomic planes. The relationship between the crystal grain size and the full width at half maximum (FWHM) of diffraction peak was deduced by Scherer for the first time, known as the Scherer equation as shown in equation (3.16). By using the Scherer equation, we can quantitatively calculate the relationship between the FWHM of diffraction peak and the crystal grain size (Venkateswarlu et al., 2014).

$$D = \frac{K\lambda}{\beta \cos\theta} \tag{3.16}$$

Where: D = Crystalline size

λ = XRD radiation of wavelength (nm)

K = Shape factor can be 0.62 - 2.08.

θ = Braggs angle in degree

β is line of broadening at FWHM in radians or measurement of the full width at half maximum of the radian peak located at any 2θ.

Dislocation density is a measure of the number of dislocations within a unit volume of the crystal. It was determined using XRD data with relate to crystalline size (Borbély & Groma, 2001; Rai et al., 2023).

$$\delta = \frac{1}{D^2} \tag{3.17}$$

Where: δ = Dislocation density in nm^{-2}

D = Crystallite size of the particles estimated from Scherer's equation.

3.3.9.2 Optical microscope (OM)

The structure of a prepared sample material surface had seen with an optical microscope Huvitz HR-300 (at ASTU, material lab). A metallurgical optical microscope was used to characterize the sintered Fe-V_2AlC-GO samples, as shown in the figure below. Four photomicrographs of the sample were taken for microstructural characterization. In this study, OM is used to examine uniformly distribution of composites.

Figure 3.11 Sample prepared for test and OM test

CHAPTER FOUR: RESULTS AND DISCUSSIONS

4.1 Introduction

The experimental results of all the test and characterizations had discussed in this chapter. This study includes a variety of analyses of several test, optimization and characterizations. The composites of iron matrix reinforced with V_2AlC max phase, (solid lubricant GO) were analyzed for density, hardness, compression, corrosion and wear test, (XRD and optical microscopy were used for characterization).

4.2 Experimental Result and Discussion

In this study density, porosity and hardness were analyzed in the first round based on the interrelation of powder metallurgy process parameters (milling time, compaction pressure and sintering temperature) at fixed reinforcement 5% of V_2AlC and 4% of GO for nine samples and optimization were performed.

4.2.1 Density of composite materials

Table 4.1 below shows the density of sintered samples for nine samples with three trials for different powder metallurgy process parameters generated by L9 orthogonal array at fixed reinforcement.

Table 4.1 Experimental density of Fe-V_2AlC-GO

Sample	Density (g/cm^3) 5% of V_2AlC			Average density
	1	2	3	
S_1	6.4248	6.8555	6.8862	6.722141
S_2	5.5009	6.9711	7.0447	6.505594
S_3	6.2278	6.7709	6.8143	6.604368
S4	6.6974	6.5995	6.6233	6.640059
S_5	7.0809	6.8095	6.7894	6.893314
S_6	6.7093	6.6661	6.7302	6.701834
S_7	7.1067	6.9168	7.0440	7.022507
S8	6.0189	6.5905	6.6388	6.416072
S_9	6.8209	6.9122	6.4138	6.715638

Figure 4.1 illustrates the experimental value of average density of developed samples based on powder metallurgy process parameters (MT, CP and ST). Generally a lower density can negatively affect the mechanical and physical properties of the final product.

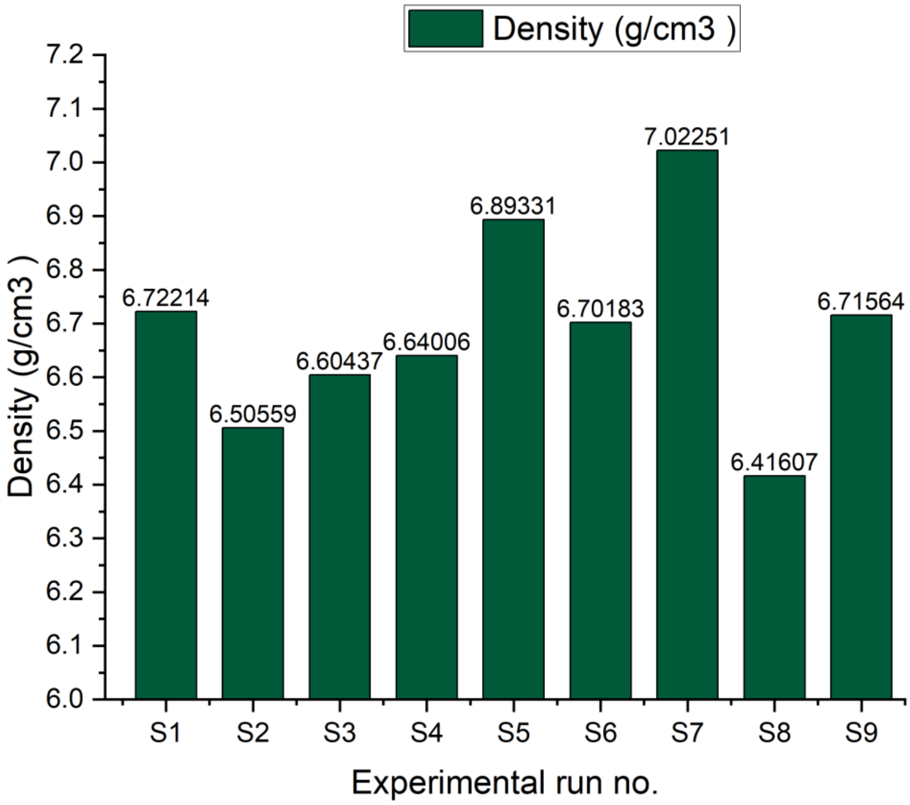

Figure 4.1 Experimental density of Fe-V2AlC-GO (5% V2AlC)

Increasing sintering temperature in powder metallurgy can initially increased density as more atomic diffusion occurs, but at very high temperatures, it can lead to reduced density due to grain growth, over-burning, and phase transformations. This effect was generally more pronounced when the sintering temperature was excessively high. From the experimental test sample fabricated through $A_1B_2C_2$ (S_7) had higher density compared with others then followed by $A_2B_2C_3$ (S_5) this indicated that the sintering temperature increased to 1100 ºC, the density decreased. This was because as the temperature raised, the thermal expansion of the particles occurs, and particles expand, resulting in larger particle sizes. Although the particles grow larger at higher temperatures, the mismatch expansion between particles could leave tiny voids between the particles (Anis et al., 2021). This condition causes greater porosity and as a result lower density.

Sample eight ($A_2B_1C_2$) had the lowest density compared with others this is due to the small compaction pressure because less force were applied to the powder particles, leading to less effective densification. The experimental test also investigated the effect of milling time on density of sintered samples (5_3, S_6 and S_9) had reduced density, sample fabricated through $A_3B_3C_2$ had higher MT, CP and moderate ST but the experimental result shows us the reduction on density due to excessive milling time. This is because prolonger milling can lead to excessive particle size reduction, creating finer particles and increasing the inner particle porosity.

4.2.2 Porosity of composite material

The porosity of fabricated composite samples, were analyzed using the Archimedes technique. It was calculated from theoretical density and experimental density using equation (3.6), as illustrated in Table 4.2. Inadequate MT, CP, and ST all contribute to increased porosity. Particle clustering adversely affects the physical/mechanical properties and microstructure of PM parts. Therefore proper milling is essential for enhanced properties (Edosa et al., 2022).

Table 4.2 Experimental porosity of Fe-V_2AlC-GO

Sample	Porosity (ϕ)			Average porosity
	1	2	3	
S_1	14.064	8.302	7.892	10.08613
S_2	26.421	6.756	5.771	12.98262
S_3	16.698	9.434	8.853	11.66144
S4	10.417	11.727	11.408	11.18404
S_5	5.287	8.917	9.186	7.796549
S_6	10.258	10.836	9.979	10.35775
S_7	4.942	7.482	5.781	6.068501
S8	19.493	11.846	11.201	14.18004
S_9	8.765	7.544	14.210	10.17311

Figure 4.2 shows the percentage of porosity within fabricated composite samples. In the figure observed that low percentage of porosity for S_7 and S_5 respectively and previously stated the density of composite material for S_7 and S_5 were higher, this indicate that porosity and density have an inverse relationship. From Table 4.2 the determined porosity values were between 6.068 (S_7) to 14.18 (S_8) this indicated more porosity was exhibited therefore, appropriate parameters selection were needed.

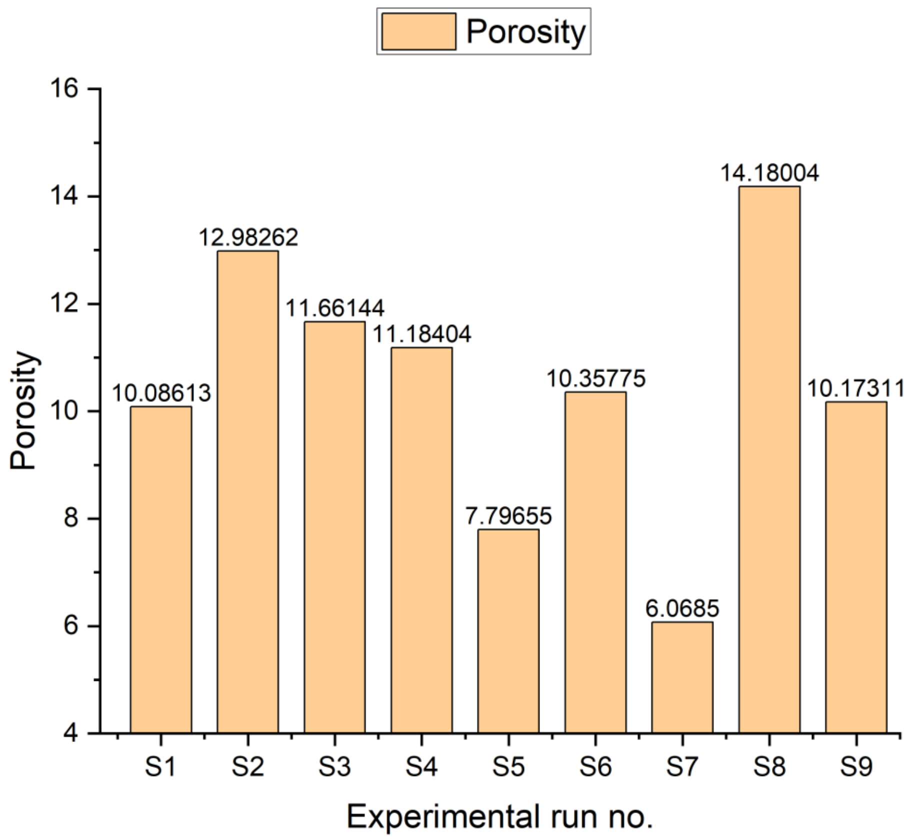

Figure 4.2 Percentage of porosity with in Fe-V2AlC (5% V2AlC)

The Figure 4.2 also illustrated the highest percentage of porosity occurred for S8 and S2 respectively this shows the process parameters used to fabricate those samples were not suitable and leads to reduction of density.

4.2.3 Hardness of composite material

The hardness of the Fe-V_2AlC-GO composite was tested using a Vickers hardness tester. Hardness tests were carried out on the composite specimen's surface in three different locations. The hardness values that were taken from the Vickers hardness test are presented in Table 4.3. The effect of process parameters on the hardness is clarified in Figure 4.3.

Table 4.3 Experimental hardness values of Fe-V_2AlC-GO composite

Sample	Vickers Hardness (HV)			Average
	1	2	3	
S_1	327.2	316.1	304.1	315.8
S_2	316.9	328.1	334.9	326.6333
S_3	325.2	323.3	312.3	320.2667
S4	425.6	422.9	441	429.8333

S_5	342.2	317.7	342.7	334.2
S_6	334	357.2	307.9	333.0333
S_7	360.7	312.3	374.3	349.1
S8	362.4	337.3	304.4	334.7
S_9	408.1	389.5	440	412.5333

From the experimental test value, the highest hardness observed for S_4 fabricated through $A_1B_3C_3$ and followed by S_9 ($A_3B_3C_2$) for both samples compression pressure was the same, for S_9 milling time increased to the highest level and sintering temperature was moderate but some reduction on hardness was occurred. On the other hand S_7 ($A_1B_2C_2$) and S_9 had the same ST but decreasing on hardness compared with S_9, this is due to the reduction of compression pressure. From previously stated the highest density observed for S_7 but the highest hardness occurred for $S_{4,}$ this indicated that distribution of particles were not uniform therefore analysis and optimization was needed to achieve optimal process parameters.

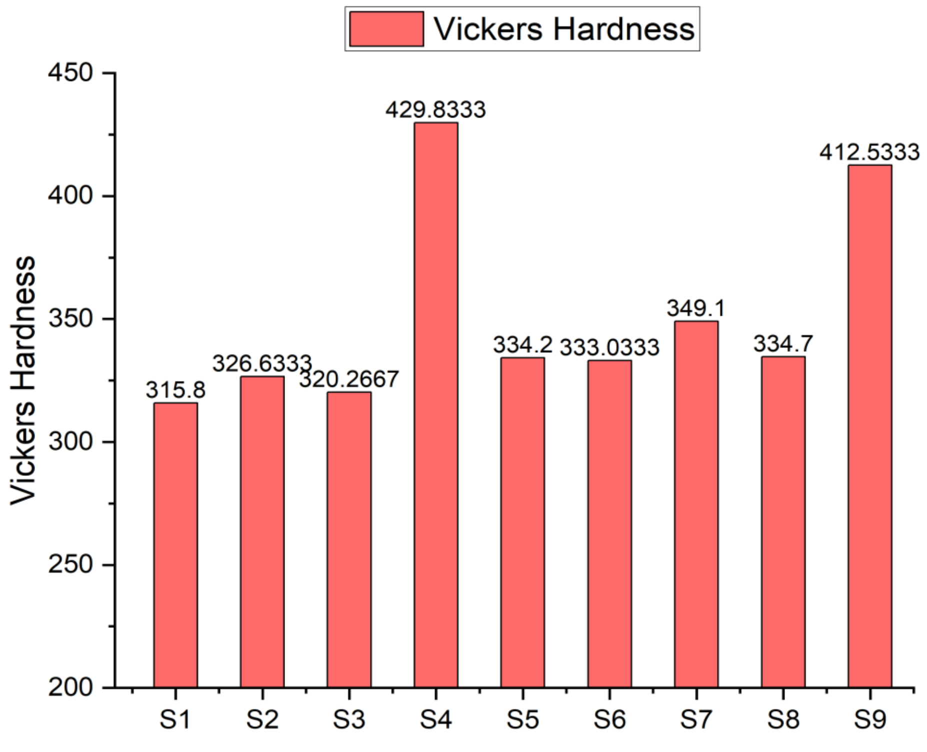

Figure 4.3 Average hardness values of Fe-V2AlC-GO composite

The Figure 4.3 also illustrated the lowest hardness occurred for S_1 ($A_1B_1C_1$) and followed by S_3 ($A_3B_2C_3$) because of low compaction pressure and sintering temperature, generally from the experiment samples fabricated with the highest level of compaction pressure had relatively higher hardness.

4.3 Optimization of Parameters using Taguchi based Grey Relational Analysis

GRA does not attempt to identify the best solution, but can be used to utilize near optimal relationships between multiple responses. In this study, GRA coupled with the Taguchi method is used to find the optimal level combination of powder metallurgy process parameter for the fabrication of composites (Hussain et al., 2020). The level at which the maximum overall Grey relational grade can be achieved is called optimal level. The GRG was utilized as a performance index and determine optimal parameter setting through mean GRG analysis at each level. The ANOVA was used to find the effect of parameters on multi-responses. Based on the finding of these analyses, optimal powder metallurgy process parameters and influential parameters on response were identified.

4.3.1 Analysis of density and porosity

In this study Taguchi based analysis method were utilized using MINITAB software, as previously stated density and porosity had invers relation. The larger the better and smaller the better criteria are used for density and porosity respectively to analyze the response of the density for each experimental run. Table 4.4 and Table 4.5 shown below described the response of signal to noise ratio.

Table 4.4 Response table for density

Level	MT	CP	ST
1	16.64	16.41	16.40
2	16.39	16.70	16.54
3	16.49	16.42	16.58
Delta	0.25	0.29	0.17
Rank	2	1	3

Table 4.5 Response table for porosity

Level	MT	CP	ST
1	-18.90	-21.14	-21.23
2	-21.05	-18.28	-19.61
3	-20.60	-21.13	-19.71
Delta	2.14	2.86	1.61
Rank	2	1	3

The response table also provides the grades of influential parameters upon the responses as tabulated above in table 4.4 and table 4.5. The compaction pressure is the first influential parameter up on density and porosity, followed by milling time, and sintering temperature. From tables, the combinations of process parameters are identified using levels of each process parameter. It is obtained as $A_1B_2C_3$ for experimental density.

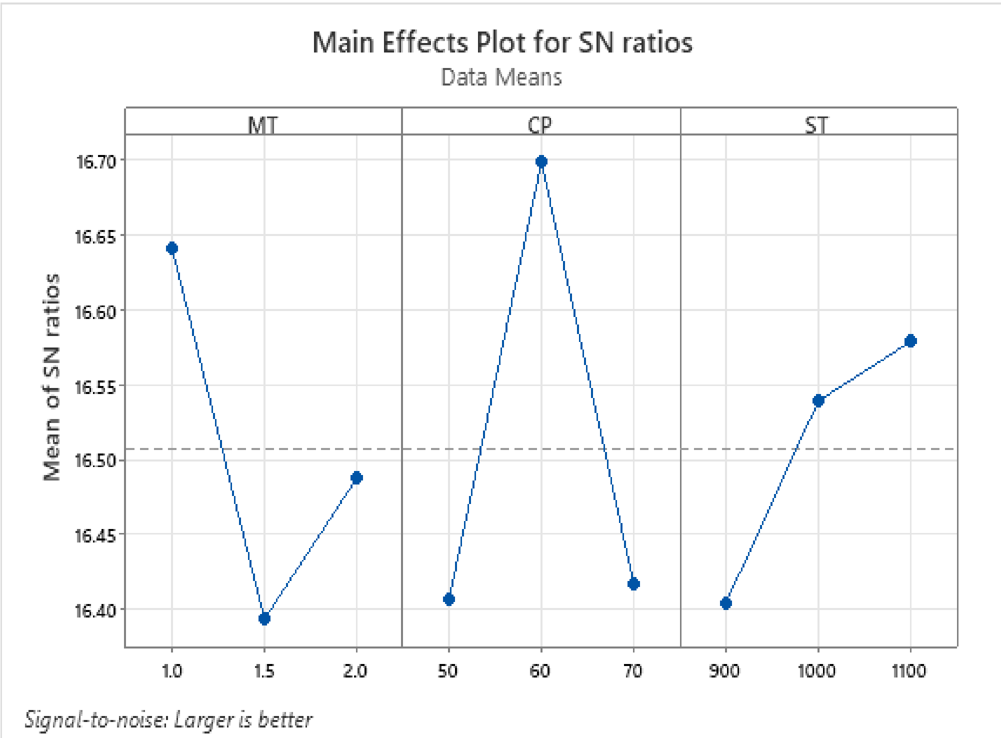

Figure 4.4 Effect of process parameters on density (S/N ratio)

The figure also illustrated that the S/N ratio increased at the first level of MT, second level of CP and third level of ST.

4.3.2 Analysis of hardness

The influence of PM process parameters on the hardness clarified using the main effect plot for S/N ratios in Figure 4.6 and larger the better criteria was used to analysis parameters. From the tabulated table the property of hardness mainly influenced by CP and followed by (ST and MT) respectively. And it reflected as the hardness property of the composites has a strong correlation with different process parameters.

Table 4.6 Response table for hardness

Level	MT	CP	ST
1	51.17	50.31	50.13
2	50.42	50.48	51.22
3	50.96	51.75	51.20
Delta	0.75	1.44	1.09
Rank	3	1	2

The Figure below illustrated the correlation of process parameters and evaluated where the higher hardness achieved, on the figure milling time at first level, compaction pressure in the third and sintering temperature in the second level was the predicted correlation PM process parameters to increase hardness.

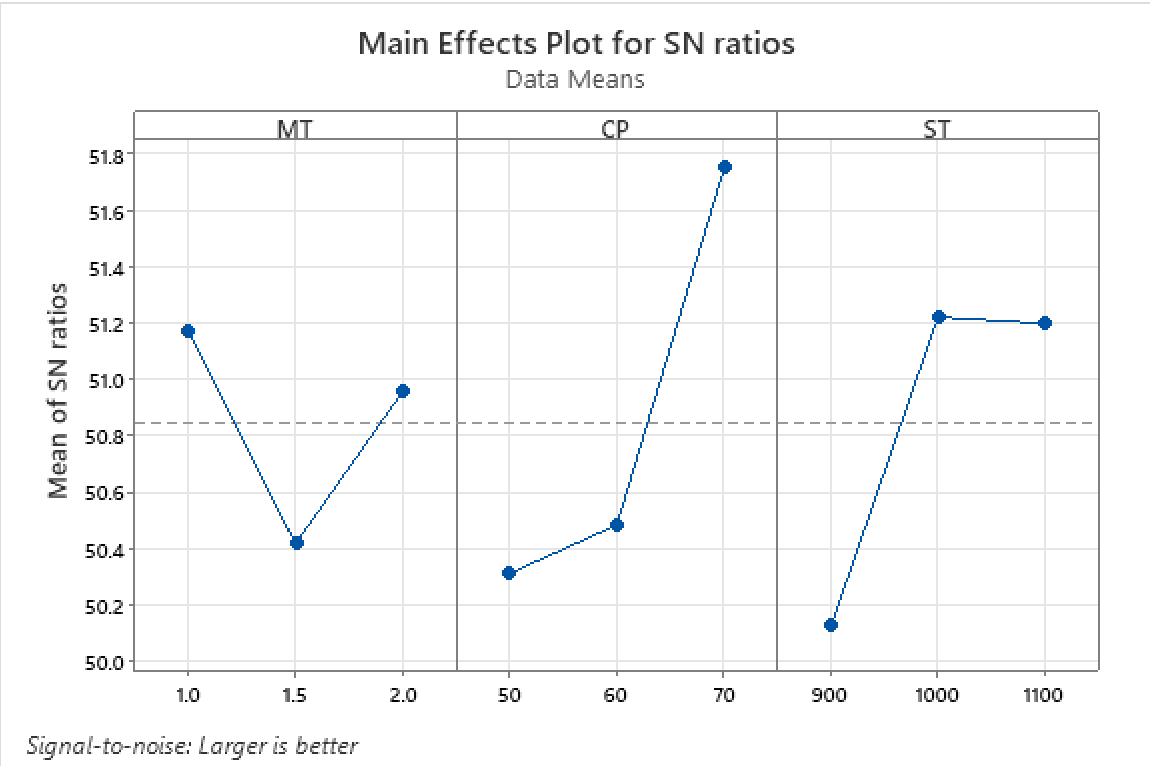

Figure 4.5 Effect of process parameters on hardness (S/N ratio)

Therefore, the optimal parameter correlation generated through Taguchi analysis for hardness is $A_1B_3C_2$.

The ANOVA table for hardness tabulated above used to identify which controllable parameter significantly affects the performance characteristic.

4.3.3 Signal to noise (SN) ratio of the experiment values

In this study, density, porosity, and hardness responses were obtained from experiments conducted using an L9 orthogonal array. Fe-5V_2AlC-GO composite with high density and hardness were desired, the higher-the-better criteria and lower-the-better criteria were applied for (density and hardness) and porosity respectively to convert the response data into the S/N ratio. The transformed density, porosity, and hardness response data into the S/N ratio are presented in Table 4.7

Table 4.7 S/N ratio of experimental responses

Sample	Experimental density	Porosity	Hardness
S_1	16.54	-20.40	49.98
S_2	16.09	-24.13	50.27
S_3	16.37	-21.72	50.11
S4	16.44	-20.98	52.66
S_5	16.76	-18.06	50.46
S_6	16.52	-20.31	50.40
S_7	16.93	-15.79	50.78
S8	16.12	-23.33	50.43
S_9	16.53	-20.49	52.28

The S/N values of density and hardness were normalized by using equation (3.10) and porosity was normalized by using equation (3.11) as tabulated in Table 4.8. All trial run data of S/N ratio were normalized to a range of 0–1.

Table 4.8 Normalized S/N ratio, GRC and GRG

Sample	Normalized S/N ratio (Y_{ij})			Grey relational coefficient (δ_{ij})			GRG (β_{ij})	Rank
	ρ	ϕ	HV	ρ	ϕ	HV		
S_1	0.532	0.553	0	0.517	0.528	0.333	0.459	9
S_2	0.000	1.000	0.111	0.333	1.000	0.360	0.564	4
S_3	0.338	0.711	0.048	0.430	0.634	0.344	0.469	7
S4	0.420	0.622	1	0.463	0.570	1.000	0.677	1

S_5	0.803	0.272	0.181	0.718	0.407	0.379	0.501	6
S_6	0.516	0.542	0.158	0.508	0.522	0.373	0.468	8
S_7	1.000	0.000	0.299	1.000	0.333	0.416	0.583	3
S8	0.032	0.904	0.167	0.341	0.838	0.375	0.518	5
S_9	0.521	0.563	0.857	0.511	0.534	0.777	0.607	2

After the S/N ratio was normalized, the grey relation coefficient (δij) was calculated using equation (3.12) to represent the relationship between the desired and actual experimental data. In situations where multiple factors need to be evaluated simultaneously, the grey relational coefficient allows for a comprehensive comparison of alternatives based on normalized data. Finally, the grey relational grade (βij) was computed using equation (3.13) to summarize the overall performance of different experimental conditions. The grey relational grade enables the integration of various parameters' performance into a single value, thereby facilitating decision-making across various criteria. The calculated normalized S/N ratio, grey relational coefficient (δij), and grey relational grade (βij) are shown in Table 4.8.

From Table 4.8 the means of the grey relational grade for each level of controllable parameters were calculated and summarized in Table 4.9, the larger the grey relational grade shown in bold.

Table 4.9 Response table for grade relation analysis

Parameters	Level 1	Level 2	Level 3	Rank(max-min)
MT	**0.573294**	0.527965	0.514736	(3)0.058558
CP	0.48163	0.518003	**0.616362**	(1)0.134732
ST	0.497711	**0.56949**	0.548794	(2)0.071779

As shown in the response table for grade relation analysis compaction pressure is the first influential parameter, followed by sintering time and milling time respectively. And also from the table the predicted process parameter is $A_1B_3C_2$. To confirm optimal parameter of powder metallurgy process parameters ANOVA was needed for grey analysis grade, the table below used to find out the contribution of process parameters. The contribution of each parameters calculated through, the ratio of sum of square each parameter by total sum of square.

Table 4.10 Results of the analysis of variance

Source	DF	Seq SS	Adj MS	F-ratio	Contribution
MT	2	1.2562	0.6281	3.64	11.42%
CP	2	7.2183	3.6092	20.90	65.63%
ST	2	2.1789	1.0895	6.31	19.81%
Residual Error	2	0.3453	0.1727		
Total	8	10.9988			

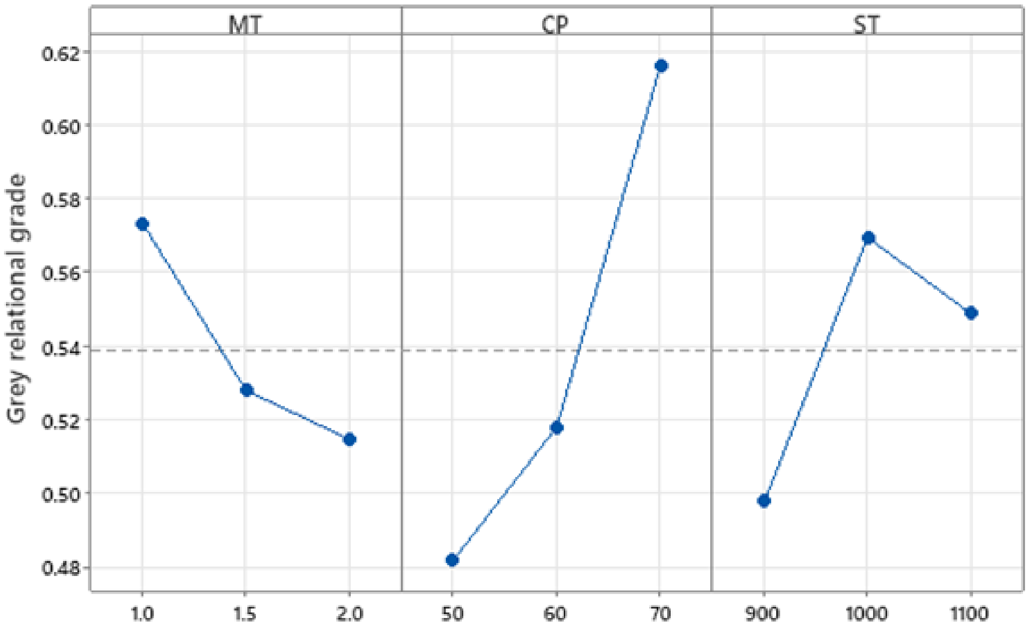

Figure 4.6 Grey relational grade graph

The results of ANOVA for the grey relational grade values are shown in Table 4.10. The results indicated that the percentage contribution of the MT, CP and ST are 11.42%, 65.63% and 19.81% respectively, the tabulated table shows as compaction pressure was the highest influential parameter, followed by sintering time and milling time and figure 4.6 illustrated at what level the desired property of density, porosity and hardness to be achieved. Therefore the optimal PM process parameters correlation identified from ANOVA analysis was $A_1B_3C_2$ which is the same with previously identified optimal parameter through response table for grey relation analysis, so the desired process parameters were confirmed based on Taguchi based GRA.

As a result the confirmation sample test were fabricated and evaluated with $A_1B_3C_2$ (powder milled for 1hr, compacted at pressure of 70Mpa and sintered at temperature of 1000 ˚C) with varying reinforcement 5%, 8%, 10%, 15% of V_2AlC and pure iron, fixed 4% of GO for all composition.

4.4 Physical and Mechanical Properties of Samples at Optimal Level

The physical and mechanical properties of sintered samples were evaluated through previously discussed procedures in chapter three. The samples sintered with varying reinforcement (5%, 8%, 10%, and 15%) of V_2AlC with 4% GO as lubricant and pure iron were fabricated at optimal parameter ($A_1B_3C_2$) for reference, denoted by S_{10}, S_{11}, S_{12}, S_{13} and S_{14} respectively.

4.4.1 Density and porosity of samples with varying reinforcement

From tabulated table and the figure illustrated below the density and porosity of samples were taken average value of three tested samples. The evaluated density values were (7.112, 7.019, 6.983, 6.691, and 7.16) in g/cm^3 for S_{10}, S_{11}, S_{12}, S_{13} and S_{14} respectively. When the percentage of reinforcement increased the density of the samples decreased due the addition of low density reinforcement compared with that of pure iron, in addition to that the percentage of porosity decreased up to 10% of reinforcement then it increases.

Table 4.11 Density, porosity and hardness value with varying reinforcement

Sample	Density	Theoretical density	Porosity	Hardness (HV)
S_{10} (5% of V_2AlC)	7.112	7.4762	4.871459	423.8
S_{11} (8% of V_2AlC)	7.019	7.3856	4.963713	468.266
S_{12} (10% of V_2AlC)	6.983	7.3252	4.671545	534.2
S_{13} (15% of V_2AlC)	6.691	7.1742	6.735246	399.733
S_{14} (pure iron)	7.16	7.6272	6.125446	230.5

For sample S_{13} porosity increased, this is due to increasing more percentage of reinforcement, as a result the volume fraction of the matrix decreases, this can lead to a reduction in the effective contact area between the base metal and the reinforcement particles, the particles are not well dispersed.

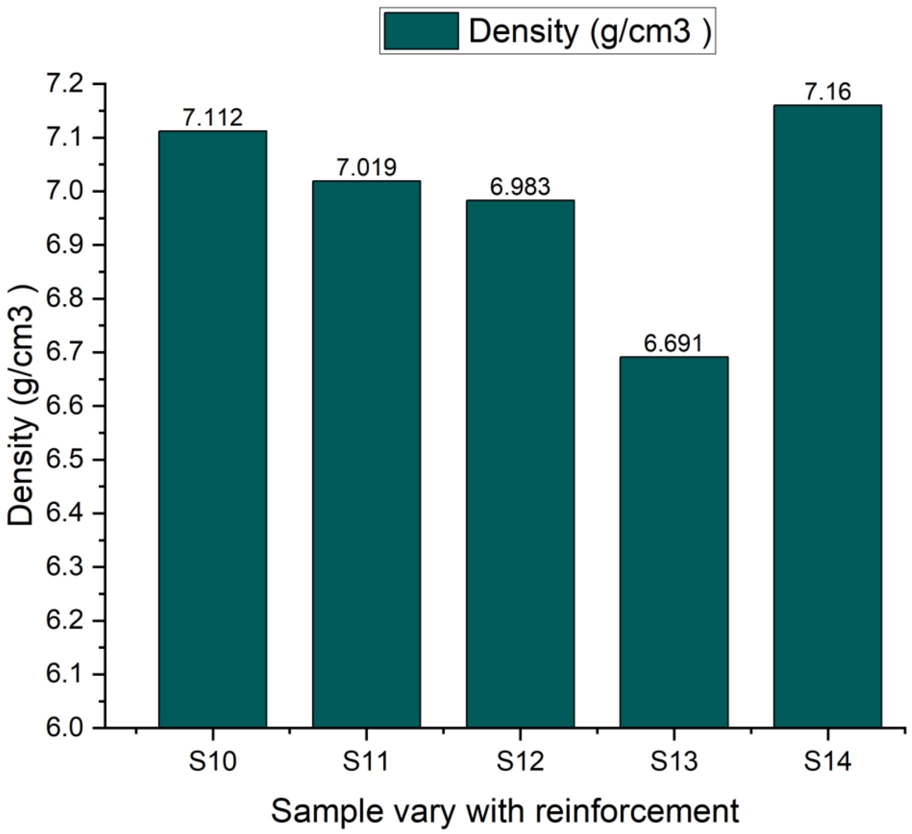

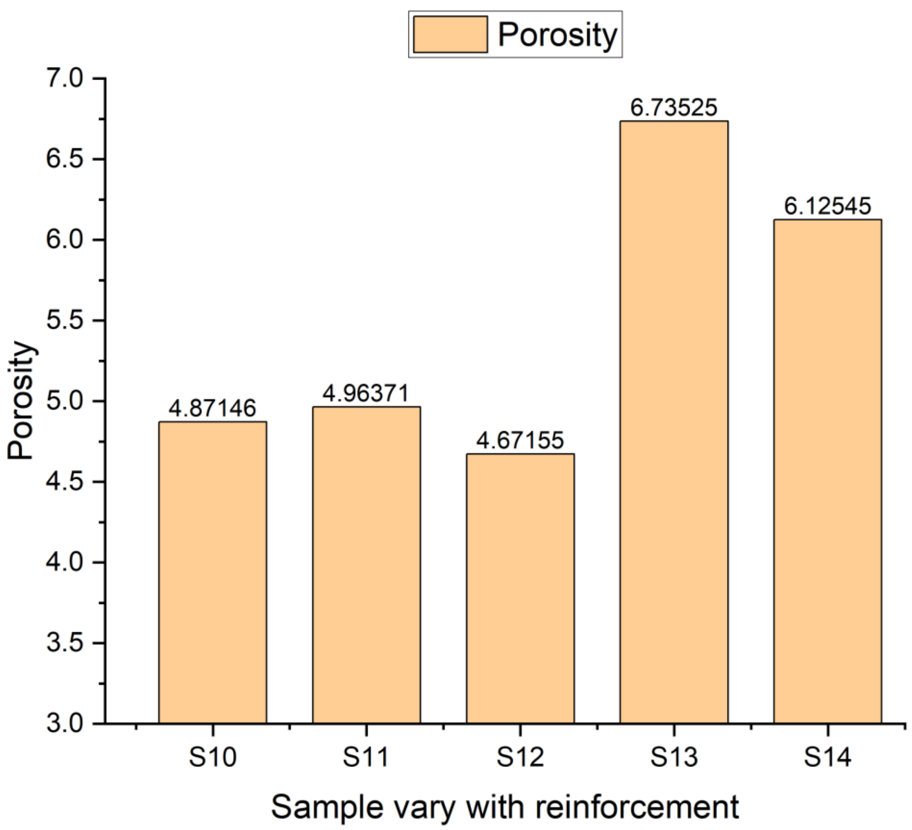

Figure 4.7 Density and Porosity value of varying reinforcement

4.4.2 Hardness property of samples with varying reinforcement

Hardness is a very important characteristic in engineering applications as it indicates a material's ability to withstand wear, friction, and others caused by external factors, therefore the developed iron-based material are used mainly in the application area which need more strength, improved the wear resistance, friction resistance, compressive strength and other related mechanical properties.

Table 4.12 Vickers hardness (10kgf) of composite material with varying reinforcement

Sample	Trial 1	Trial 2	Trial 3	Average hardness
S10	418.8	424.7	427.9	423.8
S11	465.26	467.24	472.18	468.22
S12	531.8	534.7	536.2	534.2
S13	397.1	398.4	403.7	399.733
S14	-	-	-	230.5

From the Figure illustrated below the Vickers hardness of samples (S_{10}, S_{11} and S_{12}) increased when the reinforcement increases. The hardness of S_{10} was 423.8 VH, the composition of the reinforcement were 5% V_2AlC, the same reinforcement with the first experiment. On the first experiment the highest hardness was obtained on S_4 fabricated with ($A_1B_3C_3$) process parameters on first experiment was 429.833 VH, this result with some extent greater than S_{10}. S_{10} was fabricated on $A_1B_3C_2$ optimal parameter and the desired density (7.112 g/cm^3), porosity (4.87 %) and hardness (423.8 VH). Generally improved optimal property occurred on S_{10} compared with S_4.

The highest hardness exhibited on S_{12} (534.2 VH) which was 10% of reinforcement then followed by S_{11} (8% reinforcement), the sintered sample of 15% V_2AlC (S_{13}) exhibited the reduced hardness but when compared with pure iron S_{13} exhibit improved hardness but it was smaller than S_{10} (Fe-V_2AlC-GO) at optimal parameters.

This indicated beyond 15% reinforcement of V_2AlC the desired property will not be achieve, its hardness decrease, reduction on density due to voids (pores) and also increase porosity, with high reinforcement that leads to a reduction in the effective contact area between the matrix and reinforcement particles.

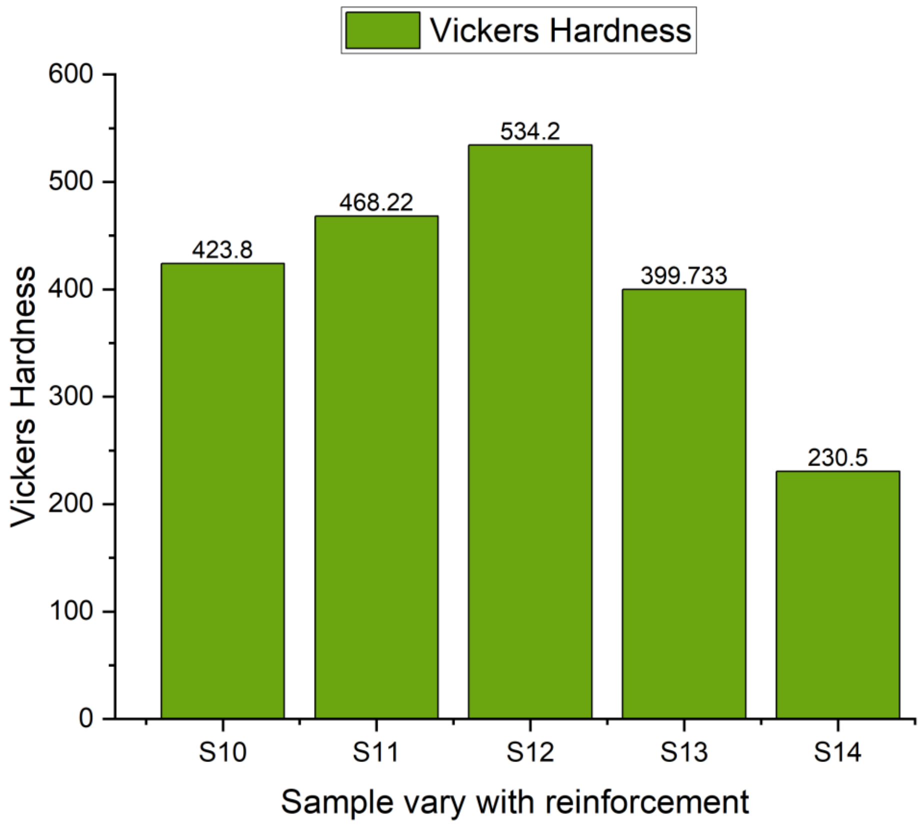

Figure 4.8 Hardness of composite material with varying reinforcement

Therefore the recommended reinforcement range between (8-12%) from the study Fe-10V_2AlC-GO composite was the acceptable improved density, porosity and hardness property.

4.4.3 Compressive strength of composite material with varying reinforcement

The compression strength test was performed on the sample produced at optimum level using UTM following ASTM Standard B925-15. The graph of applied load versus displacement during this test was shown in Figure 4.9 for sample S_{12}. The obtained maximum compressive strength was 702 MPa for S_{12} and followed by 585 MPa, 670 MPa, 570 MPa and 540 MPa for S_{10}, S_{11}, S_{13} and S_{14} respectively.

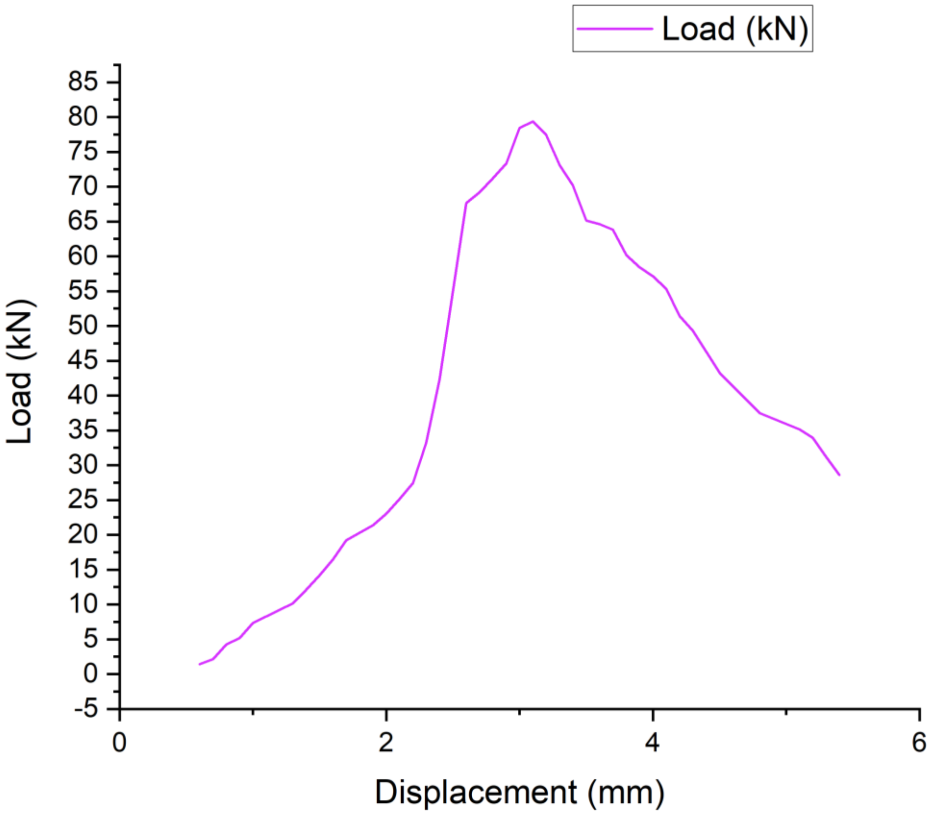

Figure 4.9 Load displacement graph of S_{12} (Fe-10V2ALC-GO)

The graph in the above demonstrates that the addition of reinforcements Fe-10V2AlC-GO improved the ability of the iron to withstand compressive loads without failure up to 702 MPa.

4.5 Corrosion Resistance of Composite Material with Varying Reinforcement

In the ASTU material lab, corrosion study on various iron composite materials in 3.5 wt% NaCl solution were performed in a biological electrochemical cell with three electrodes connected to a biological instrument Potentiostat. A NaCl electrolyte were created by dissolving 3.5% of NaCl, and 150 mL of distilled water electrolyte was taken out for each experiment. Before start the testing, the electrodes were allowed to settle for about an hour in the electrolyte solution, and the open circuit potential (OCP) were recorded as shown in (appendix-4, (A)). At a scan rate of 1 mV/sec, potentiodynamic polarization curves in the 250–250 mV region was captured for OCP. The Tafel Plot or polarization curve (corrosion potential in Y-axis, versus corrosion current in X-axis).

The Tafel estimation approach was applicable to detect potentiodynamic polarization in order to study the corrosion behavior of the manufactured samples. Calculating the rate of action of corrosion reactions can be done using the shape of the polarization curve. Tafel plots offer a different electrochemical strategy that has the benefits of quickness and relative simplicity (Olani et al., 2023).

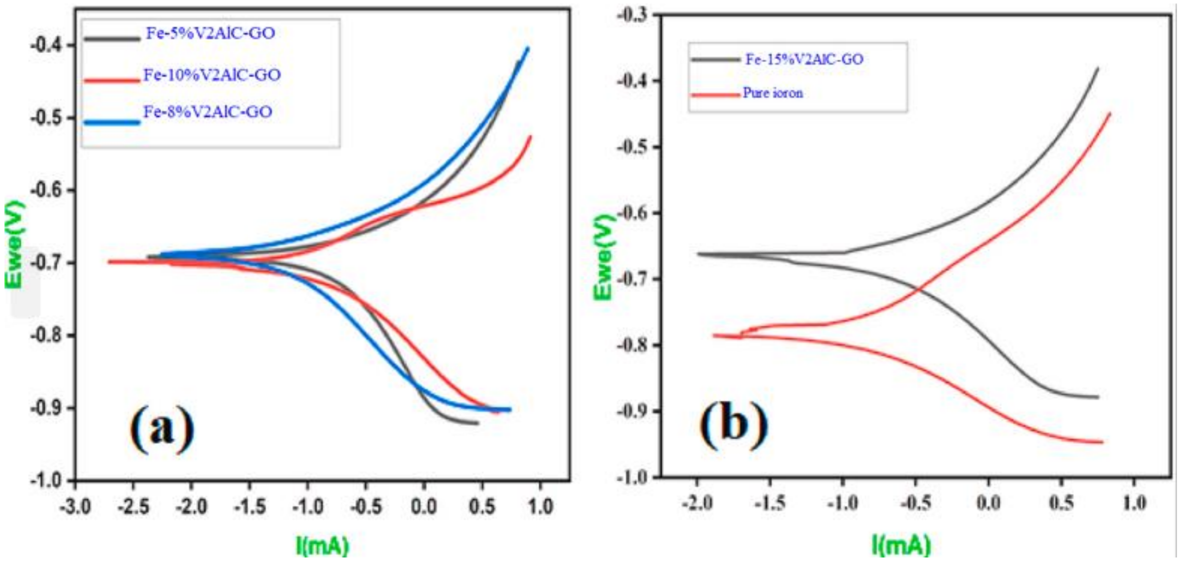

Figure 4.10 (a) and (b) Corrosion potential Ecorr for varying reinforcement

Table 4.13 Corrosion rate

Sample	Ecorr (V)	Icorr (A/cm$^{2)}$	Corrosion rate (mpy)	Protective efficiency (μp) %
S10	-0.694	657.819	1208.975	91.77
S11	-0.688	453.275	844.87	94.25
S12	-0.706	218.436	409.163	97.22
S13	-0.671	174.944	319.59	97.83
514	-0.788	8050	14705.87	0

From the table tabulated above the calculated corrosion rate based on Icorr the small corrosion rate the higher performance to resist corrosion as a result S_{13} (Fe-15%V_2AlC-GO) exhibited the higher withstand corrosion and followed by S_{12} (Fe-10%V_2AlC-GO), S_{11} (Fe-8%V_2AlC-GO), S_{10} (Fe-5%V_2AlC-GO) and S_{14} (Pure iron). From the previous study on this paper S13 exhibited bad desired property therefore S_{12} was preferable. The protective efficiency for S_{12} was 97.22 %.

4.6 Microstructural Analysis

4.6.1 Optical microscope (OM) analysis

The sample, produced at an optimal level, underwent an optical microscope test to analyze the distribution of reinforcements within the base metal. OM provides a comprehensive view of the sample's structure.

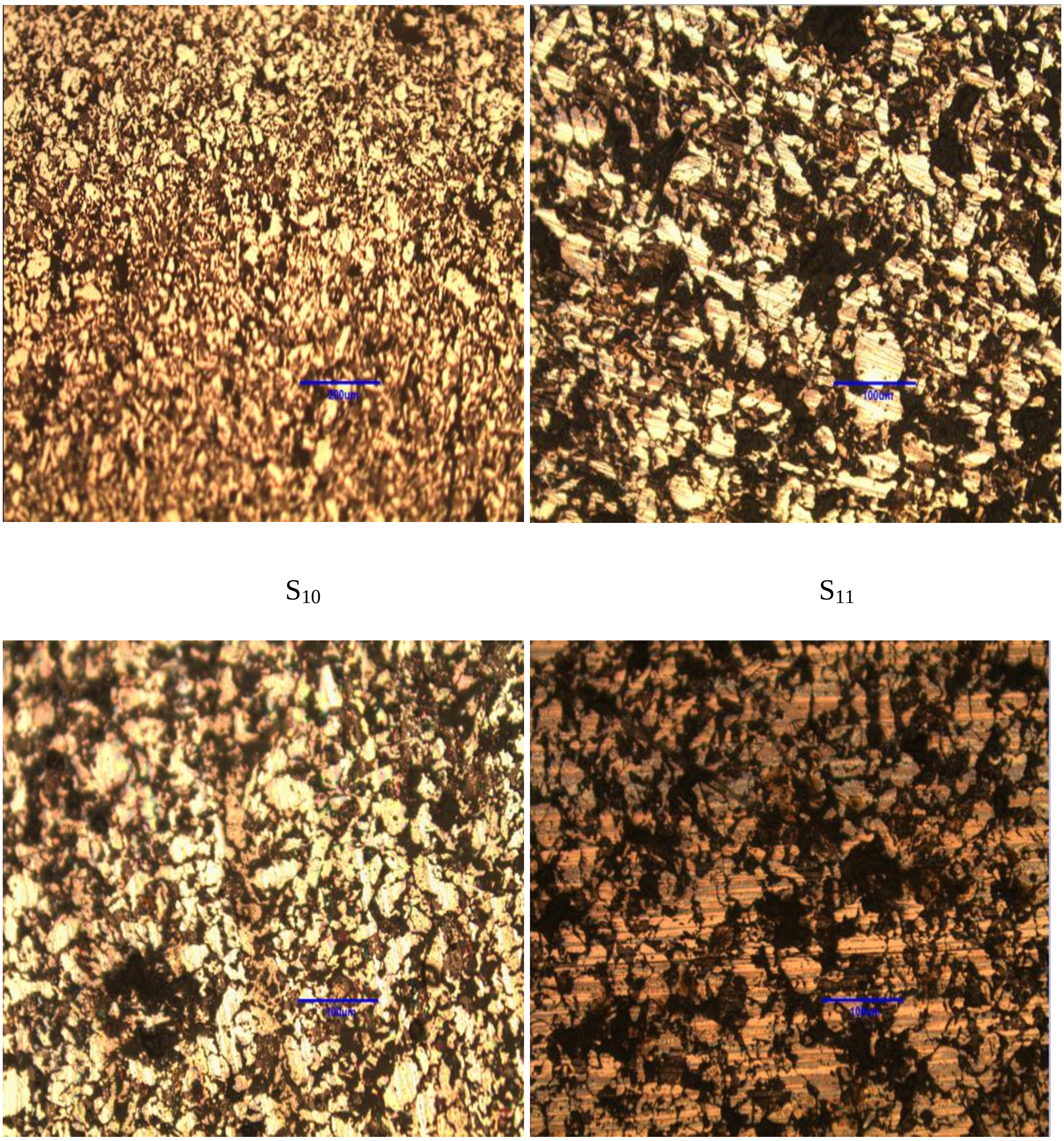

Figure 4.11 OM image of composite materials

The figure shows the OM micrograph of the composite material samples at different magnification levels. These figures reveal that the reinforcement particles were uniformly distributed throughout the base metal. Therefore, the mixing time taken, speed of mixer, and mixing method employed to mix the reinforcements and base metal were effective.

As the weight percentage of reinforcement, increase the porosity and more large grain are observed which may be due to the unreacted V_2AlC particle. From the figure S_{12} well distribution reinforcement and no more porosity. On the other hand S_{13} show more pores (voids) due to high percentage of reinforcement that leads to small contact to area between metal matrix and reinforcement.

4.6.2 X-ray diffraction (XRD) analysis

The X-ray diffraction (XRD) pattern of Fe-5V_2AlC-GO (S_{10}), Fe-8V_2AlC-GO (S_{11}), Fe-10V_2AlC-GO (S_{12}) and Fe-15V_2AlC-GO (S_{13}) were detected in angle between (10°-2θ-80°) at scan speed 3°/min. The samples' diffraction peaks were compared to XRD-JCPDS files of various materials, as shown figure (4.12). The phases present in the sample were identified by comparing the obtained angle of diffraction (2θ), intensities (I), and interplanar spacing (d) with standard reference patterns from Powder Diffraction File (PDF) databases provided by the International Centre for Diffraction Data (ICDD). The PDF card numbers of pure iron was 00-006-0696.

Table 4.14 Experimental result of XRD

Peak no.	2θ (degree)	d (Å)	IR = I/Ir	FWHM (degree)	Intensity (Counts)
1	30.2563	2.95158	4	0.5067	31
2	35.5707	2.52184	9	0.5733	78
3	35.977	2.49428	4	0.24	32
4	44.7603	2.02311	100	0.2786	859
5	65.0772	1.43214	14	0.361	116
6	82.3851	1.16962	19	0.331	167
7	82.7178	1.16575	3	0.18	29

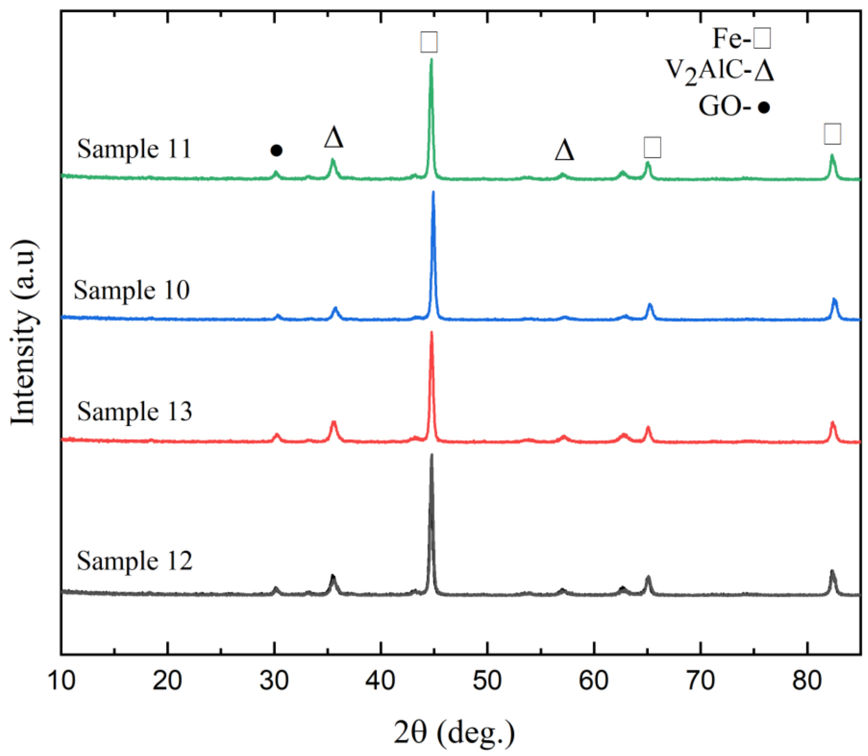

Figure 4.12 XRD Spectrum of IMMC at Different Reinforcement Content

The phase composition in the sample was verified by relative intensities. Peaks 4, 6, and 5 experienced the highest intensities, with 859, 167, and 116, respectively. Their FWHMs were also the highest and closest to one another. When compared these peaks with standard reference patterns of pure iron were close to similar. The phases for V_2AlC were identified based on published paper (Wu et al., 2018).

Crystalline sizes of sintered samples

Crystalline size calculated for S_{12} (Fe-10V_2AlC-GO) Equation (3.16) was used to determine crystalline size using the XRD data. Take K as 0.94 (recommended between (0.68-2.08) to calculate the Scherrer condition's most extreme acceptable run for Fe-V_2AlC-GO (Lee et al., 2022), and since the average value is utilized, the diffraction peak point was calculated from the XRD data as 0.15406 (°), the X-ray diffraction wavelength, and as varied as possible. There is consistency between the average grain size and the average crystalline size value of 30.46115 (nm) found in the XRD data.

Table 4.15 Crystalline size of Fe- $10V_2AlC$-GO

Parameters		Data from XRD peak analysis			
K	λ (nm)	Peak position 2θ (°)	FWHM β (°)	D(μm) D $=\frac{K\lambda}{\beta\cos\theta}$	Average (D) (nm)
0.94	0.15406	30.2563	0.5067	16.96317	31.8158
		35.5707	0.5733	15.19941	
		35.977	0.24	36.34917	
		44.7603	0.2786	32.20837	
		65.0772	0.361	27.26406	
		82.3851	0.331	33.31237	
		82.7178	0.18	61.41407	

Dislocation density

Dislocation density for is a measure of the number of dislocations within a unit volume of the crystal determined for S_{12} using equation (3.17) (0.000988 nm^{-2}).

CHAPTER FIVE: CONCLUSION AND RECOMMENDATIONS

5.1 Conclusion

In this study, two experiments of the iron metal matrix composite was successfully fabricated by incorporating V_2AlC and GO reinforcements using the powder metallurgy technique. The first experiment was 5% V_2AlC of reinforcement with 4% GO fabricated using powder metallurgy with different process parameters milling time (1, 1:30, and 2 hours), compaction pressure (50, 60, 70 MPa) and sintering temperature (900, 1000, and 1100 C˚) then hardness, density and porosity tests were analyzed, based on their result optimization was performed using Taguchi-based GRA to find the optimal parameters. After that the second experiment were performed depend on optimal parameter and fabricated four samples with vary reinforcement and additional one sample without reinforcement for comparison.

1. In this study, for powder metallurgy process parameters compaction pressure was the most influential parameter followed by sintering temperature and compaction pressure had most effect on hardness result. Milling time mainly affect the distribution of particles, sintering temperature was the significant parameter to enhance density and porosity.
2. From the first experiment with fixed reinforcement larger is better criteria was selected and the higher density were achieved 7.0225 g/cm^3 on process parameter of $A_1B_2C_2$, for smaller the better criteria for porosity the smaller porosity was achieved on $A_1B_2C_2$ (6.068) but for hardness observed higher Vickers hardness was 429.83 on $A_1B_3C_3$, this means composite material fabricated through powder mixing for one hour and compacting with 60MPa and sintered for 1000 C˚ exhibited higher density and smaller porosity on the other hand the composite material fabricated through powder mixed for one hour, compacted with 70MPa and sintered for 1100 C˚ were exhibited the higher hardness. Therefore to get the optimal parameter optimization of PM process parameters was needed and optimized using Taguchi based grey relational analysis and the optimized parameter was $A_1B_3C_2$.
3. Samples fabricated with $A_1B_3C_2$ with varying reinforcement (5%V_2AlC, 8% V_2AlC, 10%V_2AlC and 15%V_2AlC) the best physical and mechanical properties achieved on S_{12} (Fe-10 V_2AlC-GO) the achieved results were density (6.983

g/cm^3), porosity (4.671), hardness (534.2 HV) and compressive strength (702MPa). In case of corrosion S_{13} (Fe-15% V_2AlC-GO) were exhibited small corrosion rate than S_{12}, but S_{13} were not achieved desired physical and mechanical properties so S_{12} was preferable.

4. The characterization of the optimum sample using OM revealed a homogeneous reinforcement distribution. XRD analysis revealed the presence of various phases in the optimum composite. The presence of different phases (V_2AlC and GO) within iron metal matrix composite material influences its mechanical and corrosion properties.

5.2 Recommendations

Based on the research results and conclusions presented in this study, the following recommendations are suggested.

1. The addition of MAX phase V_2AlC improves the properties of iron. To achieve advanced properties, investigate iron matrix composites with a variety of reinforcements, including ceramics, alloys, and solid lubricant materials.
2. It was shown in this study that better dispersion of reinforcements leads to better mechanical, physical, and corrosion performance. So, to improve the uniformity of reinforcement distribution, investigate advanced composite manufacturing techniques.
3. The fabrication process parameters and reinforcement weight percentage for IMMC should be optimized. Because the composites developed at optimum levels exhibited improved properties.
4. From this study the recommended percentage of reinforcement between (6-12% of V_2AlC) but from this paper S_{12} (Fe-10V_2AlC-GO) achieved well properties.

REFERENCES

Almadhoni, K., & Khan, S. (2015). Review of effective parameters of stir casting process on metallurgical properties of ceramics particulate Al composites. *IOSR Journal of Mechanical and Civil Engineering*, *12*(6), 1684–2278.

Anis, A. A., Hadzley, A. B., Umar, A. A., Fairuz, M. R., Herawan, S. G., Thongkaew, K., Pembuatan, F. K., Melaka, U. T. M., Jaya, H. T., & Tunggal, D. (2021). Influence of Sintering Temperature on Density, Hardness, Shrinkage and Microstructure of Alumina-Zirconia Cutting Tool. *Int. J. Nanoelectron. Mater.*, *14*, 135–144.

Aydogmus, T. (2015). Processing of interpenetrating Mg–TiNi composites by spark plasma sintering. *Materials Science and Engineering: A*, *624*, 261–270.

Bahari, A., Sadeghi Nik, A., Roodbari, M., & Mirnia, N. (2012). Investigation the Al–Fe–Cr–Ti nano composites structures with using XRD and AFM techniques. *Sadhana*, *37*, 657–664.

Behera, M. P., Dougherty, T., & Singamneni, S. (2019). Conventional and additive manufacturing with metal matrix composites: a perspective. *Procedia Manufacturing*, *30*, 159–166.

Beshah, B., Woldegebriel, S., & Desta, G. (2015). Multi-stage and multi-response process optimization in Taguchi method. *Zede Journal*, *33*, 1–12.

Bhattacharyya, R., Iqbal, A., Gaur, T., & Gupta, P. (2021). Effect of ceramic reinforcement on the properties of iron based metal matrix nanocomposites. *Materials Today: Proceedings*, *38*, 305–312.

Bodunrin, M. O., Alaneme, K. K., & Chown, L. H. (2015). Aluminium matrix hybrid composites: a review of reinforcement philosophies; mechanical, corrosion and tribological characteristics. *Journal of Materials Research and Technology*, *4*(4), 434–445.

Borbély, A., & Groma, I. (2001). Variance method for the evaluation of particle size and dislocation density from x-ray Bragg peaks. *Applied Physics Letters*, *79*(12), 1772–1774.

Chauhan, S., Verma, V., Prakash, U., Tewari, P. C., & Khanduja, D. (2017). Studies on induction hardening of powder-metallurgy-processed Fe–Cr/Mo alloys. *International Journal of Minerals, Metallurgy, and Materials*, *24*, 918–925.

Das, A. K. (2022). Recent trends in laser cladding and alloying on magnesium alloys: A review. *Materials Today: Proceedings*, *51*, 723–727.

Das, B., Roy, S., Rai, R. N., & Saha, S. C. (2016). Development of an in-situ synthesized multi-component reinforced Al–4.5% Cu–TiC metal matrix composite by FAS technique–Optimization of process parameters. *Engineering Science and Technology, an International Journal*, *19*(1), 279–291.

Das, R., Mondal, M. K., & Pramanik, S. (2022). Strengthening Behaviour and Microstructural Properties during the Compaction of Reduced Blast Furnace Flue Dust—Fly Ash—Iron Metal Matrix Composite Fines using Powder Metallurgy Route. *Transactions of the Indian Institute of Metals*, *75*(9), 2255–2263.

Edosa, O. O., Tekweme, F. K., & Gupta, K. (2022). A review on the influence of process parameters on powder metallurgy parts. *Engineering and Applied Science Research*, *49*(3), 433–443.

Essien, U. A., & Vaudreuil, S. (2022). In-situ metal matrix composites development for additive manufacturing: a perspective. *Journal of Achievements in Materials and Manufacturing Engineering*, *111*(2), 78–85.

Girish, B. M., Siddesh, H. S., & Satish, B. M. (2019). Taguchi grey relational analysis for parametric optimization of severe plastic deformation process. *SN Applied Sciences*, *1*(8), 937.

Gotagunaki, S., Mudakappanavar, V. S., Suresh, R., & Prasad, C. D. (2023). Studies on the mechanical properties and wear behavior of an AZ91D magnesium metal matrix composite utilizing the stir casting method. *Metallography, Microstructure, and Analysis*, *12*(6), 986–998.

Gupta, P., Kumar, D., Parkash, O., & Jha, A. K. (2014). Sintering and hardness behavior of Fe-Al2O3 metal matrix nanocomposites prepared by powder metallurgy. *Journal of Composites, 2014*.

Gupta, P., Kumar, D., Quraishi, M. A., & Parkash, O. (2015). Effect of sintering parameters on the corrosion characteristics of iron-alumina metal matrix nanocomposites. *Journal of Materials and Environmental Science, 6*(1), 155–167.

Honnaiah, C., Srinath, M. S., & Lingappa, M. S. (2023). Metallographical characterization of Al-SiCP metal matrix composites processed through microwave sintering technique. *Materials Today: Proceedings*.

Hossein-Zadeh, M., Ghasali, E., Mirzaee, O., Mohammadian-Semnani, H., Alizadeh, M., Orooji, Y., & Ebadzadeh, T. (2019). An investigation into the microstructure and mechanical properties of V2AlC MAX phase prepared by microwave sintering. *Journal of Alloys and Compounds, 795*, 291–303.

Hussain, M. Z., Khan, S., & Sarmah, P. (2020). Optimization of powder metallurgy processing parameters of Al2O3/Cu composite through Taguchi method with Grey relational analysis. *Journal of King Saud University-Engineering Sciences*, *32*(4), 274–286.

Issa, S. A. M., Almutairi, A. M., Albalawi, K., Dakhilallah, O. K., Zakaly, H. M. H., Ene, A., Abulyazied, D. E., Ahmed, S. M., Youness, R. A., & Taha, M. A. (2023). Production of hybrid nanocomposites based on iron waste reinforced with niobium carbide/granite nanoparticles with outstanding strength and wear resistance for use in industrial applications. *Nanomaterials*, *13*(3), 537.

Jha, P., Gupta, P., Kumar, D., & Parkash, O. (2014). Synthesis and characterization of Fe–ZrO2 metal matrix composites. *Journal of Composite Materials*, *48*(17), 2107–2115.

Jha, P., Gupta, P., Kumar, D., & Parkash, O. (2015). Effect of sintering mechanism on the properties of ZrO2 reinforced Fe metal matrix nanocomposite. *Journal of Composites*, *2015*.

Jha, P., Kumar, D., & Mishra, V. K. (2022). Development of mathematical models to predict the density and hardness of Fe-ZrO2 composites. *Advances in Materials and Processing Technologies*, *8*(3), 3042–3056.

Karabulut, H., Erden, M. A., Karacif, K., & Gündüz, S. (2022). Investigation of the effects of SiC reinforcement ratio in iron-based composite materials on corrosion properties. *Journal of the Southern African Institute of Mining and Metallurgy*, *122*(6), 316–322.

Khazaal, S. M., Nimer, N. S. M., Szabolcs, S., & Abdulsamad, H. J. (2022). Study of manufacturing and material properties of the hybrid composites with metal matrix as tool materials. *Results in Engineering*, *16*, 100647.

Kumar, A., Vichare, O., Debnath, K., & Paswan, M. (2021). Fabrication methods of metal matrix composites (MMCs). *Materials Today: Proceedings*, *46*, 6840–6846.

Kumar, N., Bharti, A., Dixit, M., & Nigam, A. (2020). Effect of powder metallurgy process and its parameters on the mechanical and electrical properties of copper-based materials: Literature review. *Powder Metallurgy and Metal Ceramics*, *59*, 401–410.

Kumar, N., Bharti, A., & Saxena, K. K. (2020). A re-analysis of effect of various process parameters on the mechanical properties of Mg based MMCs fabricated by powder metallurgy technique. *Materials Today: Proceedings*, *26*, 1953–1959.

Kumar, N., Bharti, A., & Saxena, K. K. (2021). A re-investigation: Effect of powder metallurgy parameters on the physical and mechanical properties of aluminium matrix composites. *Materials Today: Proceedings*, *44*, 2188–2193.

Kumar, S., Singh, R., & Hashmi, M. S. J. (2020). Metal matrix composite: a methodological review. *Advances in Materials and Processing Technologies*, *6*(1), 13–24.

Kumar, V. M., & Venkatesh, C. V. (2019). A comprehensive review on material selection, processing, characterization and applications of aluminium metal matrix composites. *Materials Research Express*, *6*(7), 72001.

Kumar, Y., & Singh, H. (2014). Multi-response optimization in dry turning process using Taguchi's approach and utility concept. *Procedia Materials Science*, *5*, 2142–2151.

Kuo, Y., Yang, T., & Huang, G.-W. (2008). The use of grey relational analysis in solving multiple attribute decision-making problems. *Computers & Industrial Engineering*, *55*(1), 80–93.

Lee, M. Y., Choi, Y. J., Woo, H. J., Kim, S. W., & Lee, B. W. (2022). Microwave absorption properties of Ni0. 6Zn0. 4Fe2O4 composites with nonmagnetic nanoferrite percentages. *Ceramics International*, *48*(14), 20187–20193.

Lei, X., & Lin, N. (2022). Structure and synthesis of MAX phase materials: a brief review.

Critical Reviews in Solid State and Materials Sciences, *47*(5), 736–771.

Li, C., Li, Y., Shi, J., Li, B., Du, Y., Goei, R., Gao, Y., Shah, I. A., Zhao, S., & Tok, A. I. Y. (2022). Interfacial characteristics and wear performances of iron matrix composites reinforced with zirconia-toughened alumina ceramic particles. *Ceramics International*, *48*(1), 1293–1305.

Li, Y., Li, C., Tang, S., Zheng, Q., Wang, J., Zhang, Z., & Wang, Z. (2019). Interfacial bonding and abrasive wear behavior of iron matrix composite reinforced by ceramic particles. *Materials*, *12*(22), 3646.

Liu, R. J., Yang, L. X., Wang, Y., Liu, H. J., Zhu, S. L., & Zeng, C. L. (2021). Synthesis and characterization of submicro-sized V2AlC ceramics by a two-step modified molten salt method. *Ceramics International*, *47*(11), 16086–16093.

Mardani, A., Zavadskas, E. K., Streimikiene, D., Jusoh, A., & Khoshnoudi, M. (2017). A comprehensive review of data envelopment analysis (DEA) approach in energy efficiency. *Renewable and Sustainable Energy Reviews*, *70*, 1298–1322.

Mavhungu, S. T., Akinlabi, E. T., Onitiri, M. A., & Varachia, F. M. (2017). Aluminum matrix composites for industrial use: advances and trends. *Procedia Manufacturing*, *7*, 178–182.

Meher, B. S., Saha, R., & Chaira, D. (2021). Fabrication of MWCNTs reinforced iron metal matrix composite by powder metallurgy: Effects of wet and dry milling. *Journal of Alloys and Compounds*, *872*, 159688.

Meignanamoorthy, M., & Ravichandran, M. (2018). Synthesis of metal matrix composites via powder metallurgy route: A review. *Mechanics and Mechanical Engineering*, *22*(1), 65–75. https://doi.org/10.2478/mme-2018-0007

Mohseni-Salehi, M. S., Taheri-Nassaj, E., Babaei, A., & Soleimanzade, M. (2022). Effect of different precursors on the formation and physical properties of V2AlC MAX phase. *Journal of Alloys and Compounds*, *918*, 165588.

Mortensen, A., & Llorca, J. (2010). Metal matrix composites. *Annual Review of Materials Research*, *40*, 243–270.

Mussatto, A., Ahad, I. U. I., Mousavian, R. T., Delaure, Y., & Brabazon, D. (2021).

Advanced production routes for metal matrix composites. *Engineering Reports*, *3*(5), e12330.

Öksüz, K. E., Çevik, M., Bozdağ, A. E., Özer, A., & Simsir, M. (2014). Production of (VB) reinforced Fe matrix composites. *International Journal of Materials and Metallurgical Engineering*, *8*(8), 800–804.

Olani, M., Kumar, D., & Asrat, G. (2023). Mechanical and corrosion properties of Fe–SiC–ZrO2 hybrid composite fabricated through powder metallurgy process. *Results in Engineering*, *17*, 100866.

Onal, M., & Gavgali, M. (2017). Production of Metal Matrix Composites by in situ techniques. *J. Sci. Eng. Res*, *4*(2), 78–82.

Panda, D. (2016). *Development of Al-Fe3Al Composites by Powder Metallurgy Route*.

Parray, M. R., Khan, N. Z., & Maqbool, A. (2021). Fabrication and characterization of magnesium based surface composites with hybrid reinforcements by friction stir processing: a review. *Materials Today: Proceedings*, *46*, 6507–6512.

Paswan, S. K., Kumari, S., Kar, M., Singh, A., Pathak, H., Borah, J. P., & Kumar, L. (2021). Optimization of structure-property relationships in nickel ferrite nanoparticles annealed at different temperature. *Journal of Physics and Chemistry of Solids*, *151*, 109928.

Rai, A., Rai, P., Kumar, A., Chaturvedi, R. K., & Singh, V. K. (2023). Study of Mechanical Characteristics of Silicon Carbide Reinforced Zn-Mg Based Metal-Ceramic Composite. *Silicon*, *15*(13), 5679–5690.

Rajyalakshmi, G., & Venkata Ramaiah, P. (2013). Multiple process parameter optimization of wire electrical discharge machining on Inconel 825 using Taguchi grey relational analysis. *The International Journal of Advanced Manufacturing Technology*, *69*, 1249–1262.

Sahu, P. K., & Pal, S. (2015). Multi-response optimization of process parameters in friction stir welded AM20 magnesium alloy by Taguchi grey relational analysis. *Journal of Magnesium and Alloys*, *3*(1), 36–46.

Sahu, P. S., & Banchhor, R. (2016). Fabrication methods used to prepare Al metal matrix composites-A. *Int. Res. J. Eng. Technol*, *3*(10), 123–132.

Samal, P., Tarai, H., Meher, A., Surekha, B., & Vundavilli, P. R. (2023). Effect of SiC and WC reinforcements on microstructural and mechanical characteristics of copper alloy-based metal matrix composites using stir casting route. *Applied Sciences*, *13*(3), 1754.

Sankhla, A., & Patel, K. M. (2022). Metal matrix composites fabricated by stir casting process–a review. *Advances in Materials and Processing Technologies*, *8*(2), 1270–1291.

Sharma, D. K., Mahant, D., & Upadhyay, G. (2020). Manufacturing of metal matrix composites: A state of review. *Materials Today: Proceedings*, *26*, 506–519.

Sharma, P., Singh, K., & Pandey, O. P. (2021). Investigation on oxidation stability of V2AlC MAX phase. *Thermochimica Acta*, *704*, 179010.

Shivakumar, S. P., Sharan, A. S., & Sadashivappa, K. (2020). Experimental Investigation of Mechanical Properties of Al6061 Reinforced with Iron oxide. *IOP Conference Series: Materials Science and Engineering*, *925*(1), 12049.

Singh, A., Singh, J., Sinha, M. K., & Kumar, R. (2022). Ferrous Metal Matrix Composites Status Scope and Challenges. *ArXiv Preprint ArXiv:2204.09999*.

Singh, A., Singh, J., Sinha, M. K., & Kumar, R. (2023). Ferrous-metal matrix composites: a review on status, scope and challenges. *International Journal on Interactive Design and Manufacturing (IJIDeM)*, *17*(6), 2807–2829.

Sree Manu, K. M., Ajay Raag, L., Rajan, T. P. D., Gupta, M., & Pai, B. C. (2016). Liquid metal infiltration processing of metallic composites: a critical review. *Metallurgical and Materials Transactions B*, *47*, 2799–2819.

Tugirumubano, A., Go, S. H., Shin, H. J., Joseph, V. S., Kwac, L. K., & Kim, H. G. (2021). Magnetic and mechanical characterization of Al-MWCNT-Fe-Ni hybrid metal matrix composites. *Materials Science and Engineering: B*, *266*, 115045.

Venkateswarlu, K., Sandhyarani, M., Nellaippan, T. A., & Rameshbabu, N. (2014). Estimation of crystallite size, lattice strain and dislocation density of nanocrystalline carbonate substituted hydroxyapatite by X-ray peak variance analysis. *Procedia Materials Science*, *5*, 212–221.

Winarni, S., & Indratno, S. W. (2018). Application of multi response optimization with grey relational analysis and fuzzy logic method. *Journal of Physics: Conference Series*, *948*(1), 12075.

Wu, M., Wang, B., Hu, Q., Wang, L., & Zhou, A. (2018). The synthesis process and thermal stability of V2C MXene. *Materials*, *11*(11), 8–11. https://doi.org/10.3390/ma11112112

Yılmaz, O. (2001). Abrasive wear of FeCr (M7C3–M23C6) reinforced iron based metal matrix composites. *Materials Science and Technology*, *17*(10), 1285–1292.

Zainuri, M., & Bäßler, R. (2019). Mechanical strength and corrosion rate of aluminium composites (Al/SiO2): nanoparticle silica (NPS) as reinforcement. *Journal of Physical Science*, *30*(1), 81–97.

Zhou, Z., Liu, B., Guo, W., Fu, A., Duan, H., & Li, W. (2021). Corrosion behavior and mechanism of FeCrNi medium entropy alloy prepared by powder metallurgy. *Journal of Alloys and Compounds*, *867*, 159094.

SPECIAL ACKNOWLEDGEMENT

This research work is funded by Adama Science and Technology University under the grant number ASTU/SM-R/1083/24, Adama, Ethiopia.

APPENDIX

Appendix

S. N	Tools / Equipment	Function
1	Electronic weighing machine	To measure the weight percentage of matrix and reinforcement and weight loss during the wear test
2	Grinding and polishing	For surface finish
3	High energy ball mill/ mixer	For mixing and reducing the size of the matrix and reinforcements 4 High-temperature box furnace For sintering the green compact
4	Hydraulic pressing machine	For compacting the mixed powder materials
5	Optical microscope	For reinforcement distribution investigation
6	Potentiodynamic polarization	For corrosion test
7	Universal testing machine	For compression strength tes
8	Vickers hardness machine	For hardness test
9	XRD	For phase analyses

Experimental result of corrosion resistance test

Sample	Ecorr (V)	Icorr (A/cm^{2})	Corrosion rate (mpy)
S10	-0.694	657.819	1208.975
S11	-0.688	453.275	844.87
S12	-0.706	218.436	409.163
S13	-0.671	174.944	319.59
514	-0.788	8050	14705.87

$$\text{Corossion rate (mmpy)} = 0.00327 \times I_{corr} \times \frac{E_w}{d}$$

For sample S12

$$\text{Corossion rate (mmpy)} = 0.00327 \times 218.436 \times \frac{4}{6.983}$$

= 409.163 mpy

Hardness tested samples S_{12} with three trial

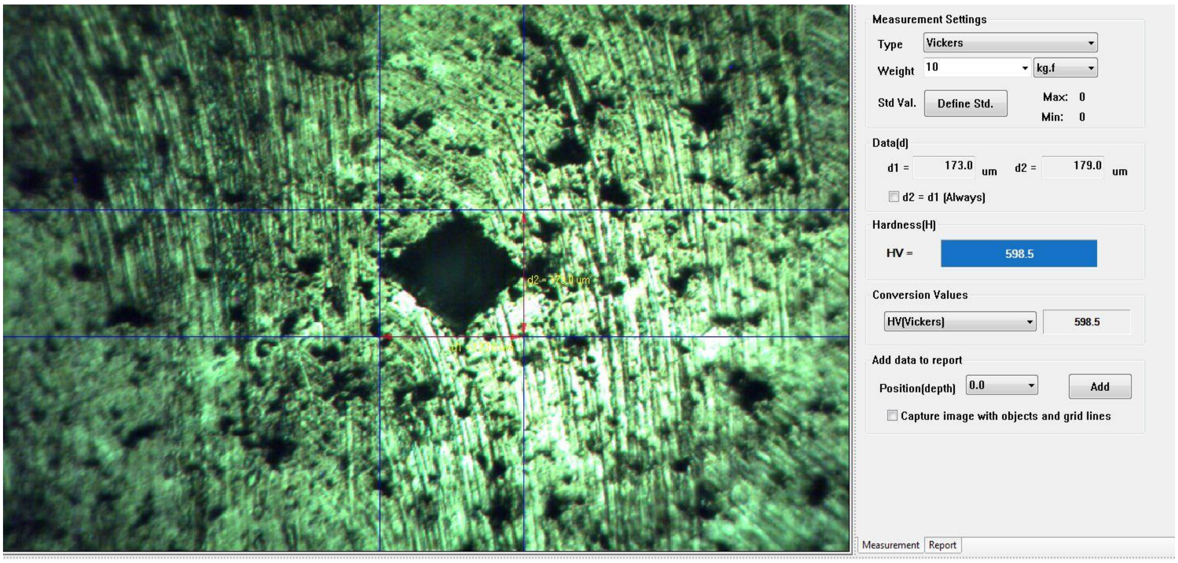

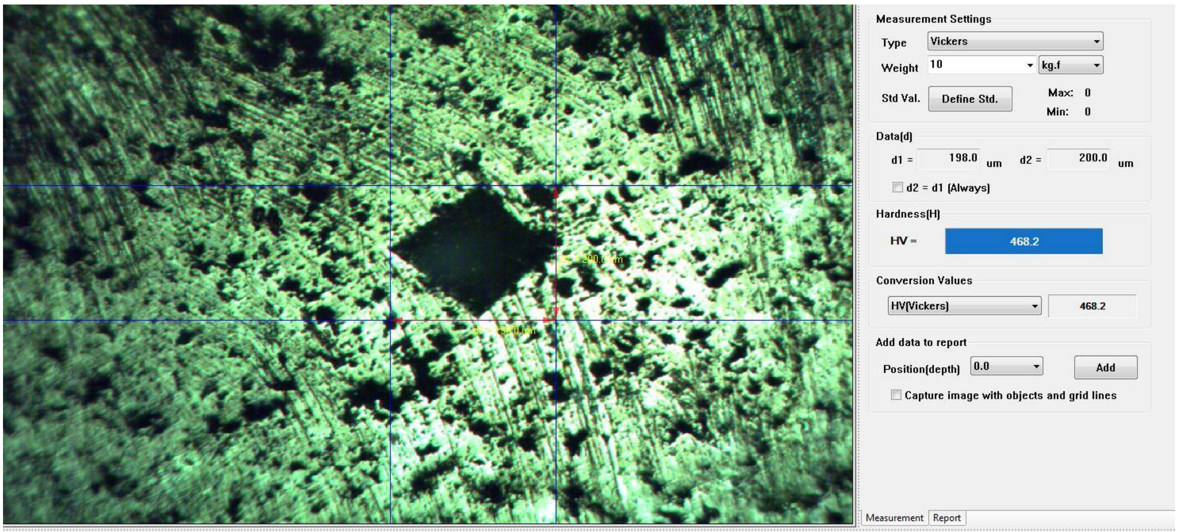

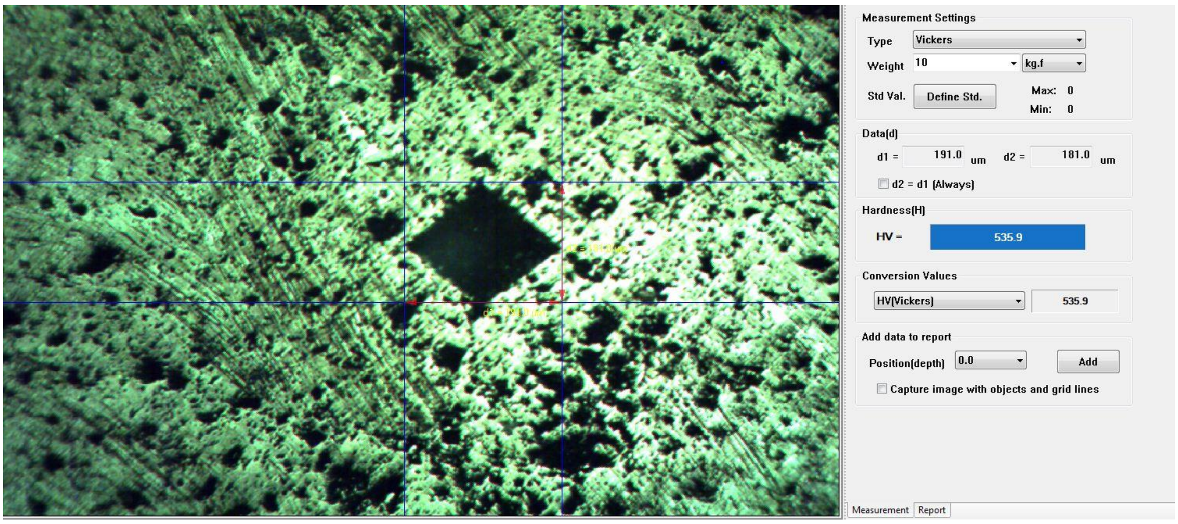

OM Images

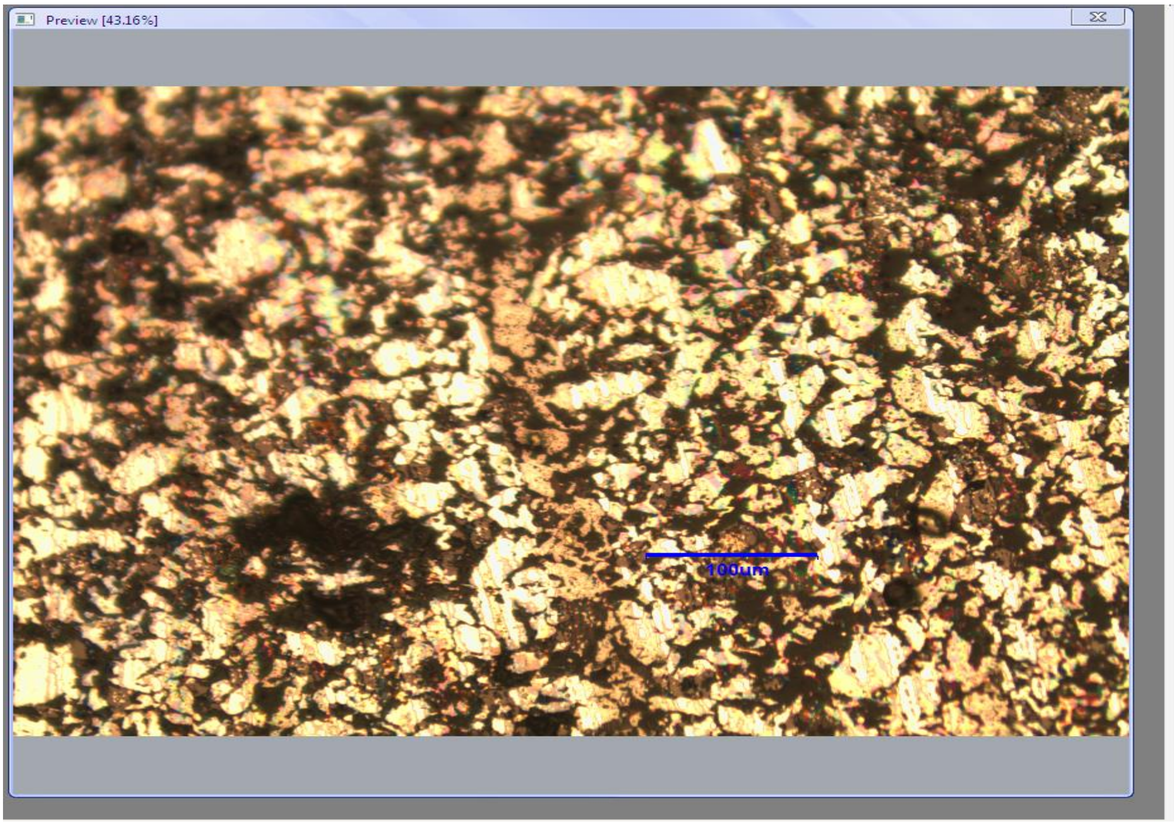
Preview [43.16%]
100um

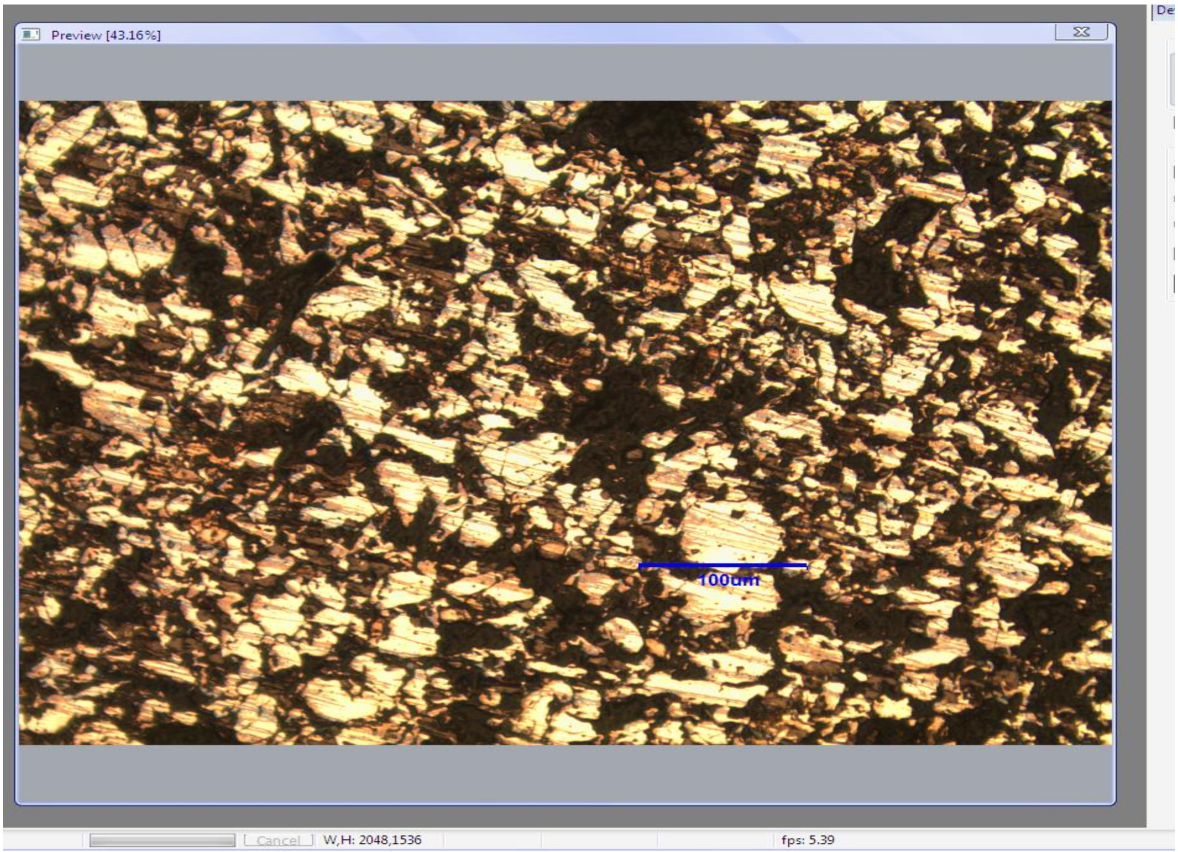
Preview [43.16%]
100um
Cancel
W,H: 2048,1536
fps: 5.39

Crystalline size of composite samples fabricated at optimal parameters

Parameters		Data from XRD peak analysis S_{10} (Fe- $5V_2AlC$-GO)			
K	λ (nm)	Peak position 2θ (°)	FWHM β (°)	D(μm) D $=\frac{K\lambda}{\beta\cos\theta}$	Average (D) (nm)
0.94	0.15406	30.3745	0.3567	24.10329	29.58743
		35.7362	0.538	16.20422	
		44.491	0.16	56.02876	
		44.916	0.2759	32.5418	
		65.226	0.4333	22.73366	
		82.5329	0.426	25.91283	
Parameters		Data from XRD peak analysis S_{11} (Fe- $8V_2AlC$-GO)			
0.94	0.15406	30.1771	0.508	16.91661	31.46149
		35.5349	0.525	16.5961	
		44.7083	0.3232	27.75859	
		57.0454	0.42	22.48465	
		62.6235	0.44	22.07246	
		62.9234	0.2934	33.15406	
		64.7228	0.1866	52.64196	
		65.0262	0.3471	28.34783	
		82.332	0.3317	33.2286	
		82.7178	0.18	61.41407	
Parameters		Data from XRD peak analysis S_{13} (Fe- $15V_2AlC$-GO)			
0.94	0.15406	30.2463	0.5933	14.48683284	21.99291451
		35.5887	0.6307	13.81645263	
		44.7555	0.3177	28.2431982	
		57.1253	0.6	15.74481356	
		62.5035	0.32	30.32954026	
		62.8034	0		
		63.0833	0.26	37.44411659	
		65.0552	0.345	28.52424547	
		82.38	0.3757	29.34703101	

Dislocation density

0.001142, 0.00101, 0.002067 in nm^{-2} for S_{10}, S_{11} and S_{13} respectively.